Control of signaling-mediated clearance of apoptotic cells by the tumor suppressor p53

HHS Public Access

Author manuscript

Science. Author manuscript; available in PMC 2017 January 05.

Published in final edited form as:

Science. 2015 July 31; 349(6247): 1261669. doi:10.1126/science.1261669.

Control of signaling-mediated clearance of apoptotic cells by the tumor suppressor p53

Kyoung Wan Yoon[1], **Sanguine Byun**[1], **Eunjeong Kwon**[1], **So-Young Hwang**[1], **Kiki Chu**[1], **Masatsugu Hiraki**[1], **Seung-Hee Jo**[1], **Astrid Weins**[2], **Samy Hakroush**[3], **Angelika Cebulla**[3], **David B. Sykes**[4], **Anna Greka**[5], **Peter Mundel**[3], **David E. Fisher**[1], **Anna Mandinova**[1,6], and **Sam W. Lee**[1,6,*]

[1]Cutaneous Biology Research Center Massachusetts General Hospital and Harvard Medical School Building 149 13th Street Charlestown MA 02129 USA

[2]Department of Pathology Brigham and Women's Hospital and Harvard Medical School Boston MA 02115 USA

[3]Division of Nephrology Department of Medicine Massachusetts General Hospital Boston MA 02114 USA

[4]Center for Regenerative Medicine and Technology Massachusetts General Hospital and Harvard Medical School Boston MA 02114 USA

[5]Department of Medicine Glom-NExT Center for Glomerular Kidney Disease and Novel Experimental Therapeutics Brigham and Women's Hospital and Harvard Medical School Boston MA 02115 USA

[6]Broad Institute of Harvard and, MIT 7 Cambridge Center Cambridge MA 02142 USA

Abstract

The inefficient clearance of dying cells can lead to abnormal immune responses, such as unresolved inflammation and autoimmune conditions. We show that tumor suppressor p53 controls signaling-mediated phagocytosis of apoptotic cells through its target, *Death Domain1*α (*DD1*α), which suggests that p53 promotes both the proapoptotic pathway and postapoptotic events. DD1α appears to function as an engulfment ligand or receptor that engages in homophilic intermolecular interaction at intercellular junctions of apoptotic cells and macrophages, unlike other typical scavenger receptors that recognize phosphatidylserine on the surface of dead cells. *DD1*α-deficient mice showed in vivo defects in clearing dying cells, which led to multiple organ damage indicative of immune dysfunction. p53-induced expression of DD1α thus prevents persistence of cell corpses and ensures efficient generation of precise immune responses.

*Corresponding author. swlee@mgh.harvard.edu.

SUPPLEMENTARY MATERIALS

www.sciencemag.org/content/349/6247/1261669/suppl/DC1

Materials and Methods

Figs. S1 to S12

Tables S1 to S25

Movies S1 to S3

During development, tissue restoration, and response to injury, numerous cells are damaged and destined to undergo cell death or apoptosis. Thus, rapid and efficient clearance of cell corpses is a vital prerequisite for homeostatic maintenance of tissue health (1, 2). Failure to clear dying cells can lead to the accumulation of autoantigens in tissues that foster diseases, such as chronic inflammatory diseases, autoimmune diseases, and developmental abnormalities (1–4). Engulfment of apoptotic cells is an active process coordinated by receptors on phagocytes and ligands on apoptotic cells (5). The exposure of phosphatidylserine (PtdSer) on the surface of dying cells is a key signal that facilitates recognition and clearance by neighboring phagocytes (6). PtdSer on apoptotic cells can be recognized directly by phagocytic receptors— such as T-cell immunoglobulin and mucin domain-1, −3, and −4 (TIM-1, TIM-3, and TIM-4); brain-specific angiogenesis inhibitor 1 (BAI1); and Stabilin-2— or indirectly via soluble bridging proteins [milk fat globule–EGF-factor 8 (MFG-E8) and complement component (C1q)] to engage in engulfment of apoptotic cells (7–13).

The p53 tumor suppressor is indispensable for maintenance of genomic integrity (14–16). p53 functions as a transcription factor that is activated by various cellular stresses and governs multiple core programs in cells, including cell cycle arrest and apoptosis (17,18). p53 has been implicated in immune responses and inflammatory diseases (19–22). Several interferon (IFN)–inducible genes—such as interferon regulatory factors 5 and 9 (*IRF5* and *IRF9*), interferon-stimulated gene 15 (*ISG15*), and Toll-like receptor 3 (*TLR3*)—are also p53 targets (20,23–25). Among others, it has been reported that the expression of forkhead box P3 (*Foxp3*), a master regulator of regulatory T cells (T_{regs}), is up-regulated by p53, and the number of T_{regs} was significantly reduced in *p53*-deficient mice (26,27). p53 also stimulates innate immunity by modulating macrophage function to non-cell-autonomously suppress tumorigenesis (28). Furthermore, although it remains unknown how p53 suppresses autoimmunity and excessive inflammation, accumulating studies have provided convincing evidence that p53 deficiency is closely associated with the development of autoimmune and inflammatory diseases in mice (21, 27,29–34).

Results

Identification of a postapoptotic target gene of p53, DD1α, an immunoglobulin superfamily receptor

Through microarray analysis of cDNA expression in EJ-p53 human bladder tumor cells with a tetracycline-regulated wild-type p53 (Wt-p53) overexpression system (35), we identified the gene encoding a transmembrane receptor, *Death Domain1*α (*DD1*α), as a downstream target gene of p53. *DD1*α mRNA and protein abundance were increased in response to genotoxic stress in a p53-dependent manner (Fig. 1A and figs. S1 and S2). The characterization of candidate p53 DNA binding consensus sequences by using reporter gene assays, chromatin immunoprecipitation–quantitative real-time polymerase chain reaction (ChIP-qPCR) and electrophoretic mobility-shift assay indicated that *DD1*α was a direct transcriptional target of p53 and that a consensus p53-binding site located at −5401 to −5420 of the *DD1*α promoter conferred p53-dependent DD1α transactivation (Fig. 1B). DD1α is a member of the immunoglobulin superfamily and is also known as Gi24 or VISTA or PD-1H

or Dies1 (36–39). The DD1α protein migrated at ~50 kD on Western blots. Treatment of cells with the glycosylation inhibitor tunicamycin resulted in migration at ~30 kD, its predicted size (fig. S3). Northern blotting of various human tissues demonstrated relatively higher expression of *DD1α* in blood leukocytes, placenta, spleen, and heart and low amounts in lung, kidney, small intestine, and brain (Fig. 1C). Analysis of public database information (http://biogps.org/#goto=genereport&id=64115) (40, 41) also indicated that DD1α is expressed in immune cells, including macrophages, dendritic cells, monocytes, and myeloid and T cells. Although we identified *DD1α* as a bona fide p53 target gene, the depletion of endogenous *DD1α* by short hairpin RNAs (shRNAs) targeting different sequences in *DD1α* mRNA did not affect the DNA damage–induced apoptotic responses (figs. S4, S5C, S6, and S7B) in various cell systems carrying Wt-p53, which suggests that *DD1α* may not function as a typical p53 target gene. DD1α has similarity with several members of the immunoglobulin superfamily with the immunoglobulin variable (IgV) domain (Fig. 1C). We sought to determine whether TIM family proteins, as well as immune checkpoint coinhibitors, programmed cell death 1 (PD-1), and programmed death-ligand 1 (PD-L1), might be regulated by p53 as seen for DD1α. The TIM family proteins, including TIM-1, TIM-2/3, and TIM-4, did not show increased expression in response to p53, but genes encoding PD-L1 and its receptor PD-1 showed increased expression in response to the p53 activator Nutlin-3 small molecule (10 μM) in MCF7 human breast cancer cells (Fig. 1D). Genotoxic stimuli also activated transcription of *PD-L1* and *PD-1* in a p53-dependent manner. We verified p53-mediated activation of PD-L1 or PD-1 expression in several p53 expression systems (Fig. 1D).

p53-induced expression of DD1α is essential for engulfment of apoptotic cells by phagocytes

TIM family molecules have an important role in phagocytosis of apoptotic cells (8, 9, 11). Because DD1α is structurally similar to TIM family proteins, we investigated whether increased abundance of DD1α induction on apoptotic cells could proceed to phagocytosis of dying cells. We depleted DD1α and p53 expression in MCF7 cells exposed to the apoptotic stimulus camptothecin (CPT) with two different *DD1α* shRNAs or *p53* shRNAs (fig. S4A). About 60% of MCF7 cells expressing sh-luciferase (control), sh-DD1α, sh-p53, or both sh-DD1α and si-p53 were apoptotic after CPT treatment (fig. S4B). We used a pH-sensitive dye (pHrodo), which emits red fluorescence only when located in the phagosome (pH ~5), to distinguish engulfed cells from unengulfed cells, and we calculated the phagocytic index (number of ingested cells per 100 macrophages) (42). To examine the functional role of DD1α or p53 in engulfment of dead cells, we used freshly isolated human monocyte–derived macrophages (hu-MDMs) and measured engulfment of CPT-treated apoptotic MCF7 cells. When control apoptotic MCF7 cells were incubated with hu-MDMs, the phagocytic index was ~50 or higher (Fig. 2A), which indicated that macrophages efficiently engulfed most of the apoptotic MCF7 cells present. However, when DD1α- or p53-depleted MCF7 cells, or MCF7 cells depleted of both, were mixed with hu-MDMs, macrophages engulfed a lower number of apoptotic cells (phagocytic index of 10 to 25 for DD1α-depleted, ~30 for p53-depleted, and 10 to 25 for both p53 and DD1α-depleted) (Fig. 2A). Reexpression of DD1α in DD1α-depleted MCF7 cells restored engulfment amounts to similar to those of control cells (Fig. 2A). ZR75-1 human breast cancer cells with Wt-p53 were also used to

carry out the phagocytosis assay. Consistent with the behavior of MCF7 cells, when apoptotic ZR75-1 cells were incubated with hu-MDMs, DD1α or p53 depletion also decreased engulfment by macrophages (fig. S5). We also used two human cancer cell lines (BxPC-3, human pancreatic cancer cell line; and Hs888. T, human osteosarcoma cell line) that had very low DD1α expression, and we found that expression of DD1α was not increased by CPT (Fig. 2B, right). Apoptotic cells of both BxPC-3 and Hs888. T were less efficiently engulfed by hu-MDMs than by DD1α-expressing cell lines, such as MCF7, ZR75-1, and A375 (human melanoma cell line) (Fig. 2B, left, and fig. S6). However, ectopic expression of DD1α-HA in BxPC-3 and Hs888. T cells restored engulfment of dead cells by macrophages, which suggested that DD1α expression was sufficient to promote apoptotic cell engulfment by phagocytes (Fig. 2B).

We further examined the effects of p53 or DD1α deficiency on the phagocytosis of apoptotic cells with genetically modified mouse cells. Thymocytes isolated from wild-type (Wt), *DD1*α$^{-/-}$, and *p53*$^{-/-}$ mice were exposed to ionizing radiation (IR) to induce apoptosis and activate DD1α expression. In Wt mouse thymocytes, but not *p53*$^{-/-}$ thymocytes, IR induced accumulation of *DD1*α mRNA expression, which indicated that the regulation of DD1α by p53 is also conserved in mice (fig. S7A). The IR-induced apoptotic responses of Wt and *DD1*α$^{-/-}$ thymocytes were comparable, but *p53*$^{-/-}$ thymocytes showed less apoptosis in response to IR. To use a similar apoptotic population of cells for each phagocytosis assay, we increased the dose of IR to *p53*$^{-/-}$ thymocytes (fig. S7B) in order to increase the proportion of apoptotic cells. About 60 to 70% of thymocytes from Wt, *DD1*α$^{-/-}$, and *p53*$^{-/-}$ mice underwent apoptosis. Such cells were incubated with bone marrow-derived macrophages (m-BMDMs) from Wt mice, and the phagocytic potential was assessed with two different methods: flow cytometry–based analysis and time-lapse image-based analysis. Measurement of the m-BMDMs with increased red pHrodo signals among total m-BMDMs by flow cytometry revealed that apoptotic *DD1*α$^{-/-}$ or *p53*$^{-/-}$ thymocytes were less efficiently engulfed by macrophages than were Wt thymocytes (Fig. 2C). Time-lapse imaging analyses with carboxy-fluorescein succinimidyl ester (CFSE)–labeled (for green fluorescence) Wt, *DD1*α$^{-/-}$ and *p53*$^{-/-}$ thymocytes, and PKH26 red-labeled phagocytic m-BMDMs showed defective phagocytosis of *DD1*α$^{-/-}$ or *p53*$^{-/-}$ thymocytes by macrophages (Fig. 2D and movies S1 to S3). Together, these data demonstrate that the p53-induced accumulation of DD1α is required for engulfment of apoptotic cells by phagocytes.

Impaired clearance of apoptotic cells in the DD1α-deficient mice

We tested whether DD1α deficiency caused defects in dead cell clearance in vivo in DD1α-deficient mice. *DD1*α$^{-/-}$ mice were generated using the F1p-Cre system, and DD1α deficiency was confirmed in vivo (fig. S8). In mice with total body exposure to IR, thymocytes undergo apoptosis and are rapidly cleared by phagocytes. Whereas Wt mice showed a decrease in overall thymic size because of dead cell removal after IR exposure, *DD1*$^{-/-}$ mice showed less of a reduction in thymic size after IR exposure (Fig. 3A, top left). Quantification of cell numbers confirmed that IR-exposed *DD1*α$^{-/-}$ mice retained a larger thymic cell population than did control mice (Fig. 3A, bottom left). We observed similar changes in the spleen, another radiosensitive organ. IR clearly decreased the spleen size and weight of Wt mice, but *DD1*α$^{-/-}$ mice showed significantly less size reduction after IR (Fig.

3B). We also examined the presence of apoptotic cells in whole mounts of thymus at different times after IR exposure, by terminal deoxynucleotidyl transferase–mediated deoxyuridine triphosphate nick end labeling (TUNEL) staining. Quantification of TUNEL-stained cells was calculated as a fraction of DAPI (4′,6-diamidino-2-phenylindole)-positive cells using an imaging analysis program. In Wt and *DD1*α$^{-/-}$ mice, irradiation of thymocytes with IR induced a similar extent of apoptosis at 3 hours (~40%) and 6 hours (more than 80%). After 6 hours, apoptotic cells in Wt thymus were rapidly cleared down to 40% at 12 hours and 20% at 18 hours. However, the clearance of apoptotic cells in DD1α$^{-/-}$ thymus was delayed, with twice as many apoptotic cells remaining in *DD1*α$^{-/-}$ thymus as in Wt thymus (Fig. 3A, right). Thus, DD1α functions in apoptotic corpse clearance in vitro and in vivo. Because apoptotic cells are typically cleared rapidly in vivo, they are rarely detectable histologically. We thus examined whether *DD1*α$^{-/-}$ mice displayed defects in scavenging apoptotic cells by TUNEL staining of tissue sections. In lymph nodes and colons, we observed 7- to 8-fold and ~17-fold increases, respectively, in TUNEL-positive cells in sections from *DD1*α$^{-/-}$ mice as compared with sections from Wt animals (Fig. 3C).

We asked whether DD1α also affected the phagocytic removal of apoptotic cells in a p53-independent manner in vitro and in vivo. Treatment of dexamethasone (Dex) induces prompt and synchronous p53-independent cell death, and the consequent removal of apoptotic cells by phagocytes can provide a quantitative experimental model of apoptotic cell clearance in vitro and in vivo (43–45). Thymocytes isolated from Wt and *DD1*α$^{-/-}$ mice were exposed to Dex or IR to induce apoptosis. The apoptotic responses by IR and Dex were comparable (fig. S9A). Dex-induced apoptotic thymocytes from Wt and *DD1*α$^{-/-}$ mice were incubated with m-BMDMs isolated from Wt mice, and the phagocytic potential was assessed via flow cytometry–based analysis. Measurement of the m-BMDMs with increased red pHrodo signals among total m-BMDMs by flow cytometry revealed that Dex-treated apoptotic *DD1*α$^{-/-}$ thymocytes were less efficiently engulfed by macrophages than were Dex-treated apoptotic Wt thymocytes (fig. S9A, bottom). Wt and *DD1*α$^{-/-}$ mice were also treated with dexamethasone intraperitoneally. Whereas Wt mice showed a decrease in overall thymic size because of dead cell removal 6 hours after Dex injection, *DD1*α$^{-/-}$ mice showed less of a reduction in thymic size after Dex injection (fig. S9B, top left). Quantification of cell numbers confirmed that Dex-treated *DD1*α$^{-/-}$ mice retained a larger thymic cell population than did control mice (fig. S9B, top right). We also examined the presence of apoptotic cells in whole mounts of thymus at different times after Dex injection, by TUNEL staining. In Wt and *DD1*α$^{-/-}$ mice, Dex treatment induced a similar extent of apoptosis at 3 hours (~ 30%) and 6 hours (more than 80%). After 6 hours, apoptotic cells in Wt thymus were cleared down to ~35% at 12 hours and ~20% at 18 hours. However, the clearance of apoptotic cells in *DD1*α$^{-/-}$ thymus was delayed, with twice as many apoptotic cells remaining in *DD1*α$^{-/-}$ thymus as in Wt thymus (fig. S9B, bottom). We observed similar changes in the spleen. A decrease in spleen size and weight was apparent in Dex-treated Wt mice, but *DD1*α$^{-/-}$ mice showed less size reduction after Dex injection (fig. S9C). We also showed that there were no obvious differences in the steady-state levels of DD1α expression in multiple tissues between Wt and *p53*-null mice (fig. S10). Thus, DD1α functions in apoptotic corpse clearance by both p53-dependent and independent ways in vitro and in vivo, and phagocytic engulfment of apoptotic cells is impaired in the absence of DD1α.

DD1α expression in macrophages is required for engulfment of apoptotic cells

DD1α is highly expressed on blood leukocytes (Fig. 1C) and in macrophages (fig. S11) and dendritic cells (37,38). Because of the expression of DD1α in phagocytes, we investigated whether DD1α expression in macrophages is also necessary for the engulfment of apoptotic cells. We used Wt- or *DD1*α-null thymocytes as prey and incubated them with Wt or *DD1*$\alpha^{-/-}$ m-BMDMs for quantification of phagocytosis analysis using flow cytometry (Fig. 4A). *DD1*$\alpha^{-/-}$ m-BMDMs were deficient in uptake of pHrodo-labeled apoptotic Wt thymocytes, as compared with Wt m-BMDMs, but showed a similarly diminished engulfment rate when DD1α-null apoptotic thymocytes were used as prey. Phagocytosis analysis of Wt- and *DD1*$\alpha^{-/-}$ m-BMDMs with synthetic beads (Fig. 4B) or bacteria (*E. coli*) (Fig. 4C) further revealed that *DD1*$\alpha^{-/-}$ m-BMDMs have no defect in phagocytic ability, which suggests that DD1α-mediated engulfment is dependent upon the presence of DD1α in apoptotic cells but that engulfment of DD1α-independent targets is not. Thus, DD1α participates on both apoptotic cells and macrophages for engulfment of apoptotic cells.

PtdSer-independent engulfment of apoptotic cells by DD1α

Dying and/or apoptotic cells expose PtdSer on the outer leaflet of the surface membrane of apoptotic cells, which is considered a primary signal recognized by PtdSer receptor of phagocytes (1, 4). Therefore, we examined whether PtdSer is a ligand of DD1α receptor by protein lipid overlay assay. When membranes, spotted with 15 different lipids, were probed with DD1α recombinant proteins purified from several hosts, such as mammalian cells (293T human embryonic kidney epithelial cells), yeast, or *Escherichia coli*, DD1α did not bind to any lipids including PtdSer (fig. S12). To determine whether the DD1α pathway is functionally sufficient for apoptotic cell engulfment independent from PtdSer signaling, we knocked down DD1α expression in both Raji human lymphoma cells defective for PtdSer exposure (42, 46) and human acute T cell leukemia Jurkat cells defective for PtdSer exposure (42, 46, 47), and we treated cells with CPT to induce apoptosis and labeled them with pHrodo dye. The apoptotic Jurkat and Raji cells were then incubated with hu-MDM, and phagocytosis was determined as described in Fig. 2. Macrophages efficiently engulfed apoptotic Jurkat cells, but a lower number of apoptotic Raji cells were engulfed, as expected (fig. S13A). When DD1α-depleted Jurkat or Raji cells were mixed with hu-MDMs, engulfment by macrophages was still decreased in DD1α-depleted Raji cells at a similar ratio seen in DD1α-depleted Jurkat cells {phagocytic index of Jurkat cells: ~38 [control knockdown (KD)] to ~16 (DD1α-depleted); phagocytic index of Raji cells: ~15 (control KD) to ~5 (DD1α-depleted)} (fig. S13A). To further confirm the PtdSer signaling-independent role of DD1α in apoptotic cell engulfment, the PtdSer-binding protein, annexin V, was used to inhibit PtdSer exposure, and then we examined phagocytic potentials in DD1α-overexpressing MCF7/DD1α-KD cells. As shown in fig. S13B, the treatment of both annexin V and antibodies (Abs) against DD1α blocking further inhibited phagocytic engulfment as compared with the treatment of annexin V or blocking Abs to DD1α. Thus, DD1α-mediated phagocytosis of apoptotic cells utilizes a different mechanism from the PtdSer pathway–initiated engulfment of apoptotic cells.

Intercellular DD1α-DD1α interaction between apoptotic cells and phagocytes mediates apoptotic cell engulfment

So far, our data suggest that both DD1α on apoptotic cells and DD1α on phagocytes are required and interdependent for the engulfment of apoptotic cells. To examine the possibility of the DD1α-DD1α homophilic interactions, we studied interactions between beads coated with soluble proteins and cell surface–expressed receptor molecules, using a DD1α-Ig fusion soluble protein (DD1α-Ig) containing the extracellular domain or control Ig proteins [TIM-1-Ig and immunoglobulin (Ig)], in 293T transfected with Wt DD1α or mutant DD1α (IgV domain-deleted). DD1α-Ig proteins (but not control Ig proteins) bound to Wt DD1α proteins expressed on the cell surface, but deletion of the IgV domain abolished this interaction, which suggests the importance of homophilic DD1α binding through the IgV domain (Fig. 5A and fig. S14). To further test whether DD1α could interact with surface DD1α molecules, we used 293T cell transfectants expressing DD1α on the cell surface and several soluble Ig fusion proteins (DD1α-Ig, PD-L1–Ig, and TIM-1-Ig) for cell surface staining. DD1α-Ig, but not PD-L1–Ig or TIM-1-Ig, bound to DD1α transfectants on the cell surface (Fig. 5B). To analyze intercellular DD1α-DD1α binding, we used cell-cell adhesion assays. In addition, U2OS human osteosarcoma cells transfected with full-length DD1α, mutant DD1α with IgV domain deletion, or empty vector were incubated with CFSE-stained MCF7 cells with DD1α overexpression (MCF7-DD1α). After thorough washing to remove unbound green cells, the binding of green-labeled MCF7 cells to U2OS cells was quantified. U2OS cells with full-length DD1α overexpression showed greater binding to green-labeled MCF7-DD1α cells than did control vector or IgV domain–deleted DD1α mutant–transfected U2OS cells, which confirmed the requirement for the IgV domain for potential intercellular DD1α-DD1α interactions (Fig. 5C). Homophilic intermolecular interaction for the DD1α receptor at intercellular junctions was further confirmed by two other experiments. Binding between DD1α-Myc and DD1α-HA was detected in lysates from cultures of 293T cells overexpressing Myc-tagged DD1α and 293T cells overexpressing HA-tagged DD1α by reciprocal coimmunoprecipitation (fig. S15A). We also performed a proximity ligation assay using Duolink in situ fluorescence assay to detect the association of DD1α-DD1α molecules between two different cell types, J774.1 (macrophage) and ZR75-1 (breast carcinoma cell). Colocalization dots (generated by overlapping fluorescence signals) were detected at intercellular junctions (fig. S15B). Further confirming the specificity of intercellular binding, DD1α-transfected Jurkat cells (Jurkat-DD1α) were labeled with either cell tracer CFSE or Far Red, whereas control Jurkat cells were labeled with Far Red. CFSE-labeled Jurkat-DD1α cells were incubated with Far Red–labeled Jurkat-DD1α cells or Far Red–labeled control Jurkat cells. DD1α-DD1α-mediated intercellular bindings were then analyzed by counting the percentage of CFSE- and Far Red–double-positive populations through flow cytometry. Incubation of differently labeled Jurkat-DD1α cell populations increased binding (~26%), but the binding between Jurkat-DD1α and control Jurkat cells was minimal (~3%) (Fig. 5D). To test whether soluble DD1α-Ig proteins compete or cooperate for intercellular DD1α-DD1α binding, we preincubated Jurkat-DD1α cells with soluble DD1α-Ig or Ig proteins. We found that exogenous treatment of DD1α-Ig modestly inhibited DD1α-DD1α-mediated intercellular binding between two differently labeled Jurkat/DD1α cell populations (Fig. 5D).

We mapped the binding region for DD1α-DD1α binding by in vitro binding analysis using glutathione *S*-transferase (GST)– and histidine (His)–fused DD1α variants and observed that the extracellular (amino acids 33–194) DD1α region or the immunoglobulin domain (37–146) bound to the His-fusion protein containing only the extracellular portion of DD1α (33–194) but not with IgV-deleted DD1α or the cytoplasmic region of DD1α, which indicated that the IgV domain is essential for DD1α-DD1α interactions (Fig. 5E). Cross-linking experiments using GST-fused DD1α variants also revealed self-association of the DD1α extracellular domain in solution (Fig. 5F, left). Cross-linked dimers were observed with the DD1α extracellular domain (33–194) variant in solution but not with the cytoplasmic region of DD1α. Dimerization of DD1α was also examined in intact cells (293T). DD1α-transfected cells were incubated with or without bismaleimidohexane (BMH), another cross-linker for covalent conjugation between sulfhydryl groups. The formation of the DD1α dimer was detected on nonreducing gels after treatment of cells with BMH (Fig. 5F, right).

We tested whether the extracellular IgV region functionally contributes to apoptotic cell engulfment with the IgV domain–deleted DD1α mutant (DD1α-ΔIgV). The full-length DD1α, mutant DD1α-DIgV, or empty control vector was transfected into DD1α-depleted MCF7 cells (fig. S16A), followed by induction of apoptosis (fig. S16B). Apoptotic MCF7 cells were incubated with hu-MDMs for phagocytosis analysis. Apoptotic MCF7 cells expressing the full-length DD1α were efficiently engulfed by human macrophages, whereas apoptotic MCF7 cells expressing DD1α-ΔIgV mutant or control vector led to diminished phagocytosis by macrophages (Fig. 5G). To elucidate the possibility of the cis-dimerization for the DD1α-DD1α interaction, we performed a proximity ligation assay using the Duolink technology to detect the association of DD1α-DD1α molecules within the same cell. Colocalization dots were detected only in 293T cells overexpressing both DD1α-HA and DD1α-Myc (fig. S17), which suggests that DD1α interacts with itself in the trans, as well as in the cis, condition. Together, these data from biochemical and cellular assays demonstrate that there is likely a homophilic intermolecular interaction of the DD1α at intercellular junctions, as well as in the cis condition, that contributes to the engulfment of apoptotic cells. Our findings demonstrate an essential role for DD1α in dead cell clearance by phagocytes as the signal on both apoptotic cells and phagocytes.

DD1α-deficient mice develop autoimmune and severe inflammatory disorder

*DD1*α-null mice are viable, born at the expected Mendelian frequency, and indistinguishable in appearance from Wt littermates at an early age (48, 49). However, at the age of 7 to 10 months, these mice show severe skin inflammation in adult female *DD1*α$^{-/-}$ mice (Fig. 6A). A majority of female *DD1*α$^{-/-}$ mice had ulcerative dermatitis and 35%, 23%, and 12% of female *DD1*α$^{-/-}$ mice showed otitis, eye-related inflammation, and seizures, respectively (Fig. 6A). Impaired clearance of apoptotic cells and accumulated corpses of dead cells can cause susceptibility to autoimmune disease (1, 3, 4). Because *DD1*α$^{-/-}$ mice showed severe skin inflammation (Fig. 6B), which is one of the clinical manifestations of systemic autoimmune disease, we examined whether *DD1*α$^{-/-}$ mice showed increased autoantibody titers. Starting at 8 to 10 months of age, the abundance of antinuclear antibodies (ANA) was increased in the sera of the phenotypically affected female *DD1*α$^{-/-}$ mice (Fig. 6C and fig. S18). Additionally, Abs to double-stranded DNA (dsDNA) were found in the serum from

*DD1*α$^{-/-}$ mice (Fig. 6C). Furthermore, total immunoglobulin G (IgG) in sera from 10-month-old phenotypically affected *DD1*α$^{-/-}$ female mice was increased to ~6-fold in comparison with that of age-matched Wt mice (Fig. 6C). One of the most commonly targeted organs in systemic autoimmune disorders is the kidney (50). Consistent with other evidence of autoimmune activity, in the renal glomeruli of *DD1*α$^{-/-}$ mice, we observed immune complex deposition identified by immunofluorescence (Fig. 6D) and diffuse mesangial expansion as shown by periodic acid–Schiff (PAS)–positive material and cellular debris (Fig. 6D). Electron microscope analysis also showed an expanded mesangium with electrondense deposits and neutrophils within capillary lumens of *DD1*α$^{-/-}$ mice (Fig. 6D). Numerous large electron-dense deposits were also observed in electron micrographs of the glomerular mesangium of *DD1*α$^{-/-}$ glomeruli (Fig. 6D). Consistent with the above kidney phenotypes, *DD1*α$^{-/-}$ mice produced large amounts of protein in their urine (Fig. 6C). Together, the *DD1*α$^{-/-}$ kidney revealed a phenotype of active glomerulonephritis with a mesangioproliferative pattern of injury and immune complex deposition. We observed extensive splenomegaly and lymphadenopathy in DD1α$^{-/-}$ mice by 10 months of age (Fig. 6E). Further histological analysis revealed extensive inflammatory infiltrates in skin and lung, and extramedullary hematopoiesis, including both erythroid and myeloid hyperplasia, was evident, which indicated a major immune dysregulated phenotype of *DD1*α$^{-/-}$ mice (fig. S19).

Inhibitory role of functional DD1α-DD1α interaction in T cell activation

Given the functional and biochemical homophilic DD1α-DD1α interaction between dead cells and macrophages, we next sought to determine whether such an interaction could also occur with naturally expressed DD1α on T cells. Thus, we used flow cytometry to assess binding of DD1α-Ig to surface receptors of CD4$^+$ T cells. DD1α-Ig bound to human CD4$^+$ T cells, but the binding of DD1α-Ig to T cells treated with blocking Abs to DD1α was decreased (fig. S20A). Moreover, this binding of DD1α-Ig to CD4$^+$ T cells purified from *DD1*α$^{-/-}$ mouse was diminished as compared with its binding to Wt-CD4$^+$ T cells (fig. S20B). Expression of DD1α on antigen-presenting cells (APCs) functions as a negative regulator or ligand of T cell response in vitro and its overexpression on tumor cells interferes with protective antitumor immunity in mice (37, 51). DD1α is also expressed on T cells and can function as a coinhibitory receptor of T cell activation (38, 49, 52). Moreover, preclinical studies with blocking Abs to DD1α enhanced antitumor T cell responses, leading to inhibited tumor growth and better survival (51).

Because intercellular DD1α-DD1α interaction is likely required for its scavenger function (Figs. 2 to 5) and DD1α is also expressed on the surface of CD4$^+$ and CD8$^+$ T cells (fig. S21), we further examined whether DD1α on CD4$^+$ T cells functions as a receptor and causes DD1α-mediated inhibition of T cell activation. DD1α-Ig protein strongly inhibited proliferation of CD4$^+$ and CD8$^+$ T cells and cytokine production stimulated by CD3-specific Abs (fig. S22) (37). CD4$^+$ and CD8$^+$ T cells from Wt or *DD1*α$^{-/-}$ mice were used for DD1α-Ig–mediated T cell inhibition experiments. Engagement of DD1α-Ig inhibited CD3 Ab–induced proliferation of CD4$^+$ or CD8$^+$ T cells (~50% inhibition). However, *DD1*α$^{-/-}$ CD4$^+$ or CD8$^+$ T cells were less sensitive to DD1α-Ig (~30% inhibition) (fig. S22), although DD1α deficiency did not prevent inhibition completely. These data indicate that potential

homophilic DD1α interactions are important for the DD1α-mediated T cell inhibitory role and that DD1α functions as a receptor on T cells. These findings indicate a role for tumor suppressor p53 in regulating expression of immune regulators, including PD-1, PD-L1, and DD1α, which suggests a potential role of p53 in immune responses.

Discussion

Our findings reveal that the tumor suppressor p53–induced expression of DD1α regulates efficient clearance of dead cells and proper immune tolerance. Although these two essential activities are seemingly interrelated, the complexity of these processes is demonstrated by the many receptors and signaling pathways involved in the recognition and removal of apoptotic cells by macrophages and stringent discrimination of self antigens from nonself antigens (1, 53, 54). We found that DD1α is a receptor that engages in homophilic intermolecular interaction or dimerization at intercellular junctions of apoptotic cells and macrophages, which is critical for the engulfment of apoptotic cells. Mice deficient in scavenger receptors develop spontaneous autoimmune disease (55–58), whereas deficiencies in dead cell clearance do not always elicit autoimmunity because these apoptotic cells in these deficiencies are still able to trigger a downstream immunosuppressive signal to inhibit autoimmunity (59, 60). In a normal immune system, phagocytic engulfment of apoptotic cells is accompanied by induction of a certain degree of immune tolerance in order to prevent self-antigen recognition (53, 61).

At age 10 to 12 months after birth, *DD1*α–deficient mice showed autoimmune phenotypes predominantly in female mice. These results imply that DD1α seems to be critical in dead cell clearance, and its loss directly affects immune tolerance. Previously reported *DD1*α knockout mice were generated by a gene-trapping approach targeting coding exon 1 (48). We achieved a Cre-mediated complete deletion of exons 2 and 3 of the *DD1*α gene, which resulted in the development of similar and yet exaggerated phenotypes with moderate to severe increases in size of certain organs and prominent formation of immune infiltrates in the skin, lung, liver, and kidney. Notably the autoimmune defects observed in the aged female *DD1*α mice were apparent even in the absence of other predisposing factors and resulted in an increased late mortality rate in females. Interestingly, the autoimmune phenotype characteristic for late-stage *DD1*α knockout animals is clearly prevalent in female mice. Importantly, similar gender bias has been previously described for various animal models of autoimmune disorders, such as SLE in which female animals are significantly more susceptible to the disease (55, 62). Also, sex hormones have been previously implicated in the development of high-affinity auto-reactive B cells (63). Epidemiological studies in humans also show extremely high (9:1) gender bias toward females for systemic autoimmune diseases (64).

The process of apoptotic-cell clearance involves extensive numbers of molecules. Based on resulting phenotypes of various knockout mice, it has been suggested that some molecules are critical for proper cell turnover during development (e.g., PSR, Beclin1, Atg5) (65–67), and other molecules are essential in the adult life, when rates of apoptosis in relevant tissues are physiologically normal during tissue homeostasis or when rates of apoptosis are accelerated under various stress stimuli (e.g., MFG-E8, TIM-4, SCARF1, C1q, CD14, Mer)

(55–58, 68, 69). Our data indicate that DD1α primarily responds to apoptotic stress and is more likely to be involved in the regulation of engulfment and phagocytosis of dead cells on the sites of extensive damage because of exogenously induced cellular toxicity. Additionally, public database information [EMAGE gene expression database (http://www.emouseatlas.org/emage/)] shows that DD1α is almost not detectable at the embryonic stage, whereas PSR or Beclin1, which are involved in cell turnover during development, are markedly expressed in the embryo (70). Therefore, DD1α deficiency leads to accumulative defects of cellular clearance over prolonged time and results in an age-dependent autoimmune phenotype, which suggests the specific role of DD1α in a stress-responsive environment.

DD1α is expressed in immune cells, including macrophages and T cells, and likely functions as a receptor through DD1α-DD1α binding at intercellular junctions. We further demonstrated that DD1α has an important role as an intercellular homophilic receptor on T cells, which suggests that DD1α is a key-connecting molecule linking postapoptotic processes to immune surveillance. DD1α also appears to inhibit T cell activation. These findings establish a concept for cancer-driven control of immune surveillance: p53-dependent genotoxic stress-mediated expression of DD1α and related immune checkpoint inhibitors, such as PD-1 and PD-L1 molecules on cancer cells, may enable their interactions with T cells in order to impose suppression of the immune response and escape from immune surveillance.

Materials and methods

Plasmids, transfection, and lentiviruses

For mammalian expression vector, full-length human DD1α cDNA was subcloned into pcDNA3.1(−) tagged with HA or Myc at the C terminus using standard procedure. Immunoglobulin V domain (amino acids 45–168)–deleted mutant DD1α-ΔIgV was generated by a PCR-mediated deletion method. For Fc-tagged soluble DD1α proteins (DD1α-Ig), the extracellular region of DD1α was cloned upstream of the mouse IgG-Fc region (DD1α-Ig) in the pCMV6-AC-FC vector (OriGene, Rockville, MD). Plasmid encoding TIM-1-Ig was a gift from Terry B. Strom (Transplant Institute, Beth Israel Deaconess Medical Center and Harvard Medical School, Boston, MA). To tag HA or Flag at the N terminus of DD1α, HA or Flag was inserted between DD1α signal peptide (SP) (1–32) and DD1α peptide (33–311), resulting in the construction of SP (1–32)–HA-DD1α (33–311) and SP (1–32)-Flag-DD1α (33–311). For recombinant DD1α deletion mutants, DD1α (33–194), DD1α (37–146), DD1α-DIgV (33–311, ΔIgV), and DD1α (215–311) were generated by PCR and subcloned into pGEX-6P-1 (GE Healthcare Life Sciences, Pittsburgh, PA). DD1α (33–194) was amplified and subcloned into pRSET vector (Invitrogen, Life Technologies, Grand Island, NY). For GST-fused p53 (93–312), p53 (93–312; DNA binding domain) was subcloned into pGEX-6P-1 (GE Healthcare Life Sciences). Transfections were performed using Lipofectamine 2000 (Invitrogen). Plasmids encoding lentivirus expressing DD1α-HA were generated by cloning DD1α-HA into pLenti CMV Neo DEST. Cells were transduced with lentivirus in the presence of polybrene. Infected cells were selected in

complete appropriate medium containing 10% fetal bovine serum (FBS) and G418 and were tested 1 week after infection.

Antibodies and additional reagents

The following Abs were used for Western blot analyses or flow cytometry analysis: p53 (DO-1, Santa Cruz), p21 (DSC60, Cell Signaling Technology, Danvers, MA), β-actin (AC-15, Sigma-Aldrich, St. Louis), His (Invitrogen), GST (B-14, Santa Cruz), HA (F-7, Santa Cruz), HA (C29F4, Cell Signaling Technology), Myc (9E10, Santa Cruz), Ab against mouse DD1α (MH5A, BioLegend), Ab against human PD-1 (J116, eBioscience), Ab against human PD-L1 (M1H1, eBioscience), CTLA4 (C-19, Santa Cruz), ICOSL (LifeSpan BioSciences), Ab against human CD14 APC (61D3, eBioscience), Ab against mouse F4/80 APC (BM8, eBioscience), Ab against mouse CD45R/B220 (RA3–6B2, eBioscience), Ab against human CD4-APC (OKT4, eBioscience), Ab against mouse CD4-APC (RM4–5, eBioscience), Ab against human CD8-APC (SK1, eBioscience) and Ab against mouse $CD8a^{+}$-APC (53–6.7, eBioscience). Rabbit polyclonal and mouse monoclonal Ab against DD1α was raised against human DD1α (amino acids 33–311) as an immunogen. Beads immobilized with Abs against HA (Roche) or Myc (9B11, Cell Signaling) were used for immunoprecipitations. Recombinant human PD-1–Ig, mouse PD-1–Ig, human PD-L1–Ig, mouse PD-L1–Ig, and control Ig proteins were from R&D Systems.

Cells and culture conditions

EJ-p53 and EJ-CAT cells (human bladder cancer cell lines) (71) were cultured in the presence or absence of tetracycline (1 μg/ml) in Dulbecco's modified Eagle's medium (DMEM) containing 10% FBS (Gibco), 100 units/ml of penicillin, and 100 μg/ml of streptomycin at 37°C (72). Human MCF7 (human breast cancer cell line), ZR75-1 (human breast cancer cell line), Saos-2 (human osteosarcoma cell line), U2OS (human osteosarcoma cell line), A549 (human lung cancer cell line), A375 (human melanoma cell line), HEK293T (human embryonic kidney epithelial cell line), Hs888, and T (human osteosarcoma cell line) cells and J774 (mouse macrophage cell line) cells were maintained in DMEM (Cellgro) supplemented with 10% FBS and antibiotics. LOX-IMVI (human melanoma cell line), BxPC-3 (human pancreatic cancer cell line), Jurkat (human acute T cell leukemia cell line), and Raji (human Burkitt's lymphoma cell line) cells were grown in Roswell Park Memorial Institute medium (RPMI) (Cellgro) supplemented with 10% FBS and antibiotics. For DD1α-overexpressing Jurkat cells, Jurkat cells infected with lentivirus carrying DD1α-HA were selected with 700 μg/ml geneticin, sorted, and subcloned. The BxPC-3 cells (73) were provided by D. Panigrahy (Beth Israel Deaconess Medical Center, Boston, MA). For treatment of DNA damage agents, cells were grown to ~50% confluency prior to exposure to DNA damage agent, CPT (0.5 to 20 μM), etoposide (25 μM), or IR (13 Gy).

shRNA and siRNA experiments

Plasmids (pLKO.1-puro) expressing shRNAs against human DD1α-1 (5′-GCAGAGACAACTTCTAAGAAT-3′; TRCN0000145473, Sigma-Aldrich) and DD1α #2 (5′-GCACGATGTGACCTTCTACAA-3′; TRCN0000140372, Sigma-Aldrich) and pLKO.1-puro Luciferase shRNA Control Plasmid DNA (Sigma-Aldrich) were purchased p53

siRNA (Validated Stealth RNAi siRNA, oligo ID: VHS40367) and control siRNA (Stealth RNAi Negative Control Low GC) were purchased from Invitrogen. shRNA plasmids and siRNAs were introduced into cells by transfection using Lipofectamine 2000 (Invitrogen) or X-tremeGENE siRNA Transfection Reagent (Roche), respectively. MCF7 or ZR75-1 cells stably expressing shRNAs were generated by selection with puromycin (1.0 μg/ml for MCF7,1.25 μg/ml for ZR75-1).

RNA analysis

RNA was prepared with TRIzol Reagent (Invitrogen) according to the manufacturer's protocol. Total RNAs of human tissues were purchased from Clontech. The RNAs were analyzed by the Northern blot analysis as described previously (74). For real-time qPCR analysis, total RNAs were extracted with the Qiagen RNeasy kit with QIAshredder. cDNA was synthesized using the iScript cDNA Synthesis Kit (Bio-Rad). Primers were as follows: For human: *DD1*α: 5′-GATGTGACCTTCTACA-AGACG-3′ and 5′-GTCCTGGAACGTGAGGTTGC-*3′; PD-1:* 5′-CCAGGATGGTTCTTAGACTCCC-3′ and 5′-TTTAGCACGAAGCTCTCCGAT-3′; *PD-L1:* 5′-TGGCATTTGCTGAACGCATTT-3′ and 5′-TGCAGCCAGGTCTAATTGTTTT-3′; *RPLP0:* 5′-CAGATTGGCTACCCAACTGTT-3′ and 5′-GGG-AAGGTGTAATCCGTCTCC-3′. For mouse: *DD1*α: 5′-GGAACCCTGCTCCTTGCTATT-3′ and 5′-TTGTA-GATGGTCACATCGTGC-3′; *Rplp0*: 5-TCGGGTCCTA-GACCA-3′ and 5′-AGATTCGGGATATGCTGTTGGC −3′. qPCR analysis was performed using an Icycler IQTM5 real-time system (Bio-Rad) with SYBER Green (Roche) for detection. Expression levels of genes analyzed by qPCR were normalized relative to levels of human *RPLP0* or mouse *Rplp0* expression.

Reporter plasmid generation and luciferase assay

A portion (1.7 kb) of the human DD1α promoter region was amplified by PCR and digested with SacI and XhoI and then was subcloned into luciferase expression vector (pGL4.21[luc2P/Puro], Promega). Transcription start site is marked as +1. For 6-kb promoter-report construct, the upstream of *DD1*α promoter from 1.7 kb to 6 kb was amplified by PCR and digested with KpnI and SacI, and then ligated into 1.7-kb *DD1*α promoter-luciferase construct. All constructs are verified by DNA sequencing. For luciferase assay, the luciferase reporter plasmids were transfected into cells. Vector encoding Renilla (pRL-TK) was also cotransfected for normalization of the transfection efficiency. The luciferase activity was determined using the Dual Luciferase Reporter Assay System (Promega).

Chromatin immunoprecipitation (ChIP)

Chromatin immunoprecipitation of IR-exposed MCF7 cells was performed following the manufacturer's protocol (Upstate). Immunoprecipitation was carried out at 4°C overnight with polyclonal Ab against p53 and mouse IgG (Santa Cruz) as a negative control. Immunoprecipitated DNA was analyzed by qPCR with the following primers.

DD1α-BS1: 5′-ATATAGCAAGACCCCACCTCTACA-3′, 5′-CACAGTGCAGCAACAAATAGAAGT-3′

DD1α-BS2: 5′-CCTCAGGCTCTGAATCTACAGT-TA-3′, 5′-GGGACAGAGACTTGTACCCTACAT-5′

p21: 5′-CTCACATCCTCCTTCTTCAG-3′, 5′-CAC-ACACAGAATCTGACTCCC-3′

The amount of immunoprecipitated DNA was normalized to inputs.

Electrophoretic mobility-shift assay

After etoposide treatment, nuclear extracts were collected from MCF7 cells using a general nuclear extraction method. Nuclear extracts (5 mg) or purified recombinant p53 was incubated with ^{32}P-labeled oligonucleotides in gel shift binding buffer (5 mM Tris-HCl at pH 7.5, 20 mM NaCl, 0.5 mM $MgCl_2$, 0.25 mM EDTA, 0.2% NP-40, 2.5% glycerol, 1 mM DTT, 20 μg/ml BSA, and 40 μg/ml poly(dI-dC). The DNA-protein complexes were resolved by electrophoresis through 5% polyacrylamide gel containing 0.5% TBE. Gels were dried and exposed to X-ray film. Unlabeled wild-type oligonucleotide or unlabeled mutant oligonucleotide was added in 100-fold excess as specific or nonspecific competitor. Oligonucleotides corresponding to the DNA binding consensus sequence for human p53 (75, 76) were used.

DD1α-BS1: 5′-GCTGGGCATGGTGGTGCAT-GCCTGTA-3′

DD1α-BS1 Mut: 5′-GCTTTTTGCAGAGGTGT-CAAAGGTA-3′

DD1α-BS2: 5′-GTTAAACTGGCTCCAGCTTG-CCTAGC-3′

p21-BS: 5′-TGTCCGGGCATGTCCGGGCATGT-CCGGG-3′

p21-BS Mut: 5′-TGTCCGGGAATTTCCGGGAA-TTTCCGGG-3′

Preparation of human and mouse macrophages

For hu-MDM, human peripheral blood mononuclear cells were prepared from normal blood obtained from the Massachusetts General Hospital blood donor center (protocol number 2012P002174). Monocytes were isolated by adhering mononuclear cells to culture plates for one hour at 37°C, after which nonadherent cells were removed by washing. The remaining cells were >95% CD14 positive. Adherent cells were then incubated in DMEM/F12 medium plus 10% FBS, 1% penicillin-streptomycin for 7 days to allow terminal differentiation of monocytes to macrophages (77). For mouse bone marrow–derived macrophages (m-BMDM), femurs and tibias were harvested from 5- to 6-week-old mice and the marrow was flushed and placed into a sterile suspension of PBS. The bone marrow suspension was cultured in DMEM/F12 medium plus 10% FBS, 1% penicillin-streptomycin-glutamine with 40 ng/ml recombinant murine macrophage colony-stimulating factor (M-CSF, Peprotech). Six days later, more than 90% of the adherent cells were CD11b positive and 80% of the cells were F4/80 positive.

Generation of apoptotic cells

Apoptosis of human cancer cells was induced by CPT (0.5 to 20 μM). To generate apoptotic thymocytes, thymocytes isolated from mice were exposed to the indicated dose of IR with

constant cell concentration of 1.0×10^6 thymocytes/ml. For phagocytosis assays, apoptotic cells were labeled with pHrodo or CFSE (carboxyfluorescein diacetate succinimidyl ester) (Invitrogen). Cells were used when 60 to 70% of cells were apoptotic, as defined by annexin V–positive and propidium iodide-negative staining or TUNEL staining by flow cytometry.

Phagocytosis assay

For flow cytometry analysis of phagocytosis, 2.0×10^5 BMDMs were plated in the 24-well plate 1 day before the phagocytosis assay. Next day, the cells were starved for 30 min with DMEM/F12 containing 2% FBS and incubated with fluorescently labeled targets, such as 4.0×10^6 pHrodo (Invitrogen)-stained apoptotic thymocytes, 1 mg/ml pHrodo Red *E. coli* BioParticles (Invitrogen), or 2-μm carboxylate-modified latex beads (Invitrogen) in 150 μl of the uptake buffer (DMEM/F12 containing 2% FBS, 0.2% penicillin-streptomycin). After incubation for the indicated time, the cells were extensively washed with cold PBS, trypsinized and resuspended in cold medium containing 1% NaN_3, and analyzed by flow cytometry. Forward and side-scatter parameters were used to distinguish unengulfed targets from phagocytes. The data were analyzed using FlowJo software. Fluorescent signal–positive BMDMs were considered to be phagocytes engulfing targets (78). For time-lapse image analysis of phagocytosis, CFSE (Invitrogen)–labeled apoptotic thymocytes were added to BMDM with 1:5 ratio (BMDM:thymocyte). The individual BMDMs were monitoredbytime-lapse confocal microscopy imaging (Nikon Eclipse Ti and Zeiss LSM 510), with images being taken at 1- to 2-min intervals. For image-based analysis of phagocytosis of human cancer cells, human monocyte-derived macrophages (MDMs) were prepared from human peripheral blood and incubated with pHrodo-labeled apoptotic cancer cells with 1:10 to 1:15 ratio (MDM: cancer cell). Two hours after coincubation, wells were washed thoroughly with cold serum-free RPMI five times and examined under a fluorescence microscope (Nikon Eclipse Ti or Zeiss AxioObserver.Z1) using bright field or Texas Red filter set. The phagocytic index was calculated using the following formula: phagocytic index = number of ingested cells/(number of macrophages/100), as described previously (79). At least 400 macrophages were counted per well.

Generation and genotyping of DD1α knockout mice

A targeting vector for the mouse *DD1*α gene was engineered by InGenious Targeting Laboratory, Inc. (Stony Brook, NY). In brief, a PGK-neomycin cassette flanked by loxP and FRT sites was inserted downstream of exon 3. A third loxP site was inserted upstream of exon 2. The targeted iTL BA1 (C57BL/6 × 129/SvEv) hybrid embryonic stem cells containing the linearized construct were microinjected into C57BL/6 blastocysts. Germline transmission was achieved by back-crossing chimeras to wild-type C57BL/6 mice. To generate the whole-body *DD1*α knockout mice, $DD1\alpha^{floxneo}$; mice were first bred with β-Actin/Flp mice (The Jackson Laboratory; catalog no. 003800) to remove the PGK-neomycin cassette and then bred with EIIa-Cre mice (The Jackson Laboratory; catalog no. 003724). Mice with DD1α heterozygous allele ($DD1\alpha^{+/-}$) were backcrossed with C57BL/6J mice for at least seven generations before being intercrossed to generate mice homozygous for the null allele ($DD1\alpha^{-/-}$). Routine genotyping was achieved on genomic DNA isolated from tail snips of mice with three primers to identify wild-type and null alleles: P1, 5′-TCCTTGTGCAGGACAGAGTT-3′; P2, 5′-CTAATGGCACAGCAGGGACT-3′; and

P3,5′-CAACAAATCACGGTGGAGTG-3′. All animal experiments were approved by the Subcommittee on Research Animal Care of Massachusetts General Hospital (protocol no. 2005N000022).

Analysis of apoptotic cell clearance in vivo

Four- to 5-week-old Wt and *DD1*α$^{-/-}$ mice were exposed to *6.6* Gy of IR or intraperitoneally injected with 250 μg dexamethasone as described previously (44, 45). At the indicated time points after exposure of IR or injection of dexamethasone, the mice were euthanized and thymuses and spleens were harvested. For quantification of total number of thymocytes in thymus, thymocytes were resuspended with PBS supplemented with 5% FBS. To monitor the TUNEL-positive apoptotic cells in thymus, 6-μm cryosections of whole thymuses were stained using the In Situ Cell Death TMR Red kit and DAPI according to manufacturer′s instructions (Roche). Whole-thymus images were obtained using an automated image stitching method under fluorescence microscope (Olympus FSX100). To quantify the clearance of TUNEL-positive cells, the percentage of TUNEL-positive cells was determined by the percentage of TUNEL-positive cells per DAPI-positive cells using an imaging analysis program (CellSens Dimension, Olympus).

Mouse serologic and urine analysis

The levels of total IgG, ANA, and ant-dsDNA in mouse serum were determined by enzyme-linked immunosorbent assay according to the manufacturer's instructions (Bio-Rad) with mouse serum at a dilution of 1:10 to 1:50. For immunofluorescent analysis of ANA, HEp-2 slides were used. The images were analyzed by fluorescence microscope (Olympus FSX100). For mouse urine analysis, 24 hours albuminuria was measured using metabolic cages. Of note, mice were fed a 5% sucrose drinking solution during the 24 hours analysis in the metabolic cages. Urine (10 μl) was analyzed by SDS-PAGE and Coomassie blue staining. Bovine serum albumin (0.25, 0.5, 1.0, 2.5, and 5.0 μg) served as standard. Signals were quantified using ImageJ software (NIH). Resulting values of the 5 multiplication of the "size of the area" and the "mean gray value" of each albumin standards were used for construction of a standard curve and its associated mathematical function. Values were translated into albumin concentrations and extrapolated to 24-hour urine volume.

Histology and transmission electron microscopy

Organs were fixed by retrograde vascular perfusion with 4% paraformaldehyde in PBS, removed, and immersed in the same fixative for a maximum of 2 days until further processing for histology, immunohistochemistry, or transmission electron microscopy (TEM), as previously described (80). For immunocomplex analysis, frozen sections were used. 4 μm paraffin-processed formalin-fixed tissue sections were stained with Periodic Acid Schiff (PAS) or hematoxylin/eosin (H&E). Images were taken with an Olympus BX53 microscope with DP72 camera and processed using Adobe PhotoShop software. Ultra-thin 80-nm sections of resin-embedded kidney tissue were mounted on copper grids, treated with uranyl acetate and lead citrate, and examined by a pathologist (A.W.) in a blinded fashion using a JEOL 1010 transmission electron microscope (Tokyo, Japan).

Homophilic interaction assay

Protein A/G–purified DD1α-Ig proteins or Ig proteins (control) were covalently coupled to 6 mm blue carboxylated microparticles as recommended by the manufacturers (Polyscience, Inc.). 293T cells were transfected with the plasmids expressing full length DD1α, DD1α-ΔIgV, or control empty vector as indicated amount per well of six-well culture plates for 24 hours. The transfected cells were incubated with the Ig protein–coated beads in PBS containing 2% FBS at room temperature. After 30 min, unbound beads were washed with cold PBS and cell monolayers in culture media examined under an inverted microscope, and the binding was determined by measuring the optical density (O.D.) at 492 nm (81).

In situ proximity ligation assay

The assay was performed with the use of a Duolink using PLA Technology (Sigma-Aldrich). J774.1 macrophages and ZR75-1 breast cancer cells were transfected with plasmids encoding DD1α-HA or DD1α-Myc, respectively, for 24 hours. The transfected cells were trypsinized and cocultured on slide glasses in six-well culture plates. After 24 hours, cells were fixed, permeabilized, blocked, and then incubated with rabbit HA–specific Ab and mouse Myc–specific Ab at 4°C overnight. The cells were then subjected to an in situ proximity ligation assay with PLA probes, according to the manufacturer's protocol. All images were taken with a Nikon Eclipse Ti confocal microscope and processed using Adobe Photoshop software with minimal adjustment of brightness or contrast.

In vitro binding assay

His-fused DD1α (33–194) and GST-fused DD1α variants were purified from bacteria using Ni-NTA agarose (Life Technologies) or glutathione-Sepharose beads (GE Healthcare Life Sciences), respectively. For binding of His-DD1α (33–194) to Ig fusion proteins (DD1α-Ig, PD-1–Ig, or Ig), Ig-fused proteins were immobilized on protein A/G agarose. The His-fused DD1α (33–194) protein was incubated at 4°C for 4 hours in a binding buffer containing 20 mM HEPES, pH 7.4, 100 mM NaCl, 5 mM $MgCl_2$, 5 mM $CaCl_2$,1 mM DTT, 0.1% NP-40, and 100 μg/ml BSA with GST-fused proteins immobilized on glutathione-agarose beads or Ig-fused proteins immobilized on protein A/G. The bound His-fused protein was eluted from the beads and analyzed by SDS-PAGE and Western blot using His-specific Ab.

Protein lipid overlay assay

Membrane lipid strips (Echelon Bioscience) prespotted with 15 different biologically active lipids, at 100 pmol per spot, were purchased. Nonspecific binding of membranes was blocked by incubation for 18 hours with 3% BSA in TBS-T (50 mM Tris at pH 7.4, 0.5 M NaCl, and 0.1% Tween-20). After blocking, membranes were incubated for 2 hours with 2 μg/ml of soluble recombinant proteins, such as DD1α-Ig purified from mammalian cell, DD1α-His purified from yeast, His-DD1α purified from bacteria, and TIM-1-Ig, and then were washed and incubated with indicated Abs, followed by incubation for 1 hour with a horseradish peroxidase–labeled secondary Ab. Binding was detected by chemiluminescent detection.

T cell activation assay

The cell culture plates were coated with CD3-specific Ab (OKT3, eBioscience for human T cells; 145-2C11, eBioscience for mouse T cells) and various concentrations of DD1α-Ig or PD-L1–Ig. The amount of Ig protein was kept constant at 10 mg/ml by the addition of control Ig protein. Mouse $CD4^+$ and $CD8^+$ T cells were purified from splenocytes freshly isolated from mice using $CD4^+$ T Cell Isolation Kit II, mouse or $CD8a^+$ T Cell Isolation Kit II, mouse (Miltenyi Biotec). Purity was confirmed to be over 90% by flow cytometry. The T cells were labeled with 1 μM CFSE, quenched by cold FBS, and incubated in plates coated with CD3-specific Ab and Ig proteins. On day 2 after stimulation, supernatant was collected, and cytokines were assayed by ELISA. On day 3, cells were stained with Ab against CD4-APC (RM4–5, eBioscience for mouse $CD4^+$ T cells) or Ab against CD8-APC (53–6.7, eBioscience for mouse $CD8^+$ T cells) and then analyzed for CFSE dilution by flow cytometry.

Binding assay of Ig fusion proteins to T cells

Purified human $CD4^+$ T cells from freshly isolated PBMCs were stimulated by plate-bound CD3-specific Ab (5 μg/ml) for 3 days, collected, and then preincubated with 100 μg/ml DD1α-specific or control mouse IgG1 Ab for 30 min. Cells were then washed and incubated with 30 μg/ml DD1α-Ig or control Ig proteins (Fc portion; human IgG1; R&D Systems) for 30 min. After washing once with PBS, cells were incubated with antihuman IgG (5 μg/ml), cross-absorbed against mouse Ig (Southern Biotech), and washed twice with PBS. The bound Ig fusion proteins were analyzed by flow cytometry (82, 83).

Statistical analysis

Statistics were calculated using Prism 6.0 software (GraphPad Software). For analysis of statistical difference between experiments involving two groups, a Student's two-tailed *t* test was applied. A one-way analysis of variance (ANOVA) was applied for statistical analysis of three or more groups. Significance was defined when *P* values were <0.05.

Supplementary Material

Refer to Web version on PubMed Central for supplementary material.

Acknowledgments

We thank members of the Cutaneous Biology Research Center of MGH, J. H. Lee, J. Park, M. Kashiwagi, J. Seavitt, S. Ezell, A. Gurkar, T. Namba, and M. Choo for helpful suggestions on experiments and C. Ford and T. Woo for technical assistance. We also thank A. Sharpe and G. Freeman for precious advice, guidance during the study, and generous reading of the manuscript. This paper is dedicated to the memory of Victor Fung We also thank T. Strom for TIM family protein constructs and Z. Wang for the Protein Core from MGH. S.H. was supported by a research stipend from the Deutsche Forschungsgemeinschaft (HA 6334/1-1) and currently is in the Department of Pathology University Medical Center Göttingen Göttingen Germany. AC was supported by MD student fellowship stipends from Boehringer Ingelheim Fonds The work was partially funded by NIH grants CA149477 CA142805, CA80058, S10RR027673, DK57683, DK062472, DK091218, and DK093378.

REFERENCES AND NOTES

1. Nagata S, Hanayama R, Kawane K. Autoimmunity and the clearance of dead cells. Cell. 2010; 140:619–630. pmid: 20211132. [PubMed: 20211132]

2. Elliott MR, Ravichandran KS. Clearance of apoptotic cells: Implications in health and disease. J Cell Biol. 2010; 189:1059–1070. pmid: 20584912. [PubMed: 20584912]
3. Muñoz LE, Lauber K, Schiller M, Manfredi AA, Herrmann M. The role of defective clearance of apoptotic cells in systemic autoimmunity. Rheumatology. 2010; 6:280–289. pmid:20431553. [PubMed: 20431553]
4. Nagata S. Apoptosis and autoimmune diseases. Ann. N. Y. Acad. Sci. 2010; 1209:10–16. pmid: 20958310. [PubMed: 20958310]
5. Poon IK, Lucas CD, Rossi AG, Ravichandran KS. Apoptotic cell clearance: Basic biology and therapeutic potential. Nat. Rev. Immunol. 2014; 14:166–180. pmid: 24481336. [PubMed: 24481336]
6. Fadok VA, et al. Exposure of phosphatidylserine on the surface of apoptotic lymphocytes triggers specific recognition and removal by macrophages. J. Immunol. 1992; 148:2207–2216. pmid: 1545126. [PubMed: 1545126]
7. Park D, et al. BAI1 is an engulfment receptor for apoptotic cells upstream of the ELMO/Dock180/Rac module. Nature. 2007; 450:430–434. pmid: 17960134. [PubMed: 17960134]
8. Kobayashi N, et al. TIM-1 and TIM-4 glycoproteins bind phosphatidylserine, and mediate uptake of apoptotic cells. Immunity. 2007; 27:927–940. pmid:18082433. [PubMed: 18082433]
9. Miyanishi M, et al. Identification of Tim4 as a phosphatidylserine receptor. Nature. 2007; 450:435–439. pmid: 17960135. [PubMed: 17960135]
10. Park SY, et al. Rapid cell corpse clearance by stabilin-2 a membrane phosphatidylserine receptor. Cell Death Differ. 2008; 15:192–201. pmid: 17962816. [PubMed: 17962816]
11. DeKruyff RH, et al. T cell/transmembrane Ig and mucin-3 allelic variants differentially recognize phosphatidylserine and mediate phagocytosis of apoptotic cells. J. Immunol. 2010; 184:1918–1930. pmid: 20083673. [PubMed: 20083673]
12. Hanayama R, et al. Identification of a factor that links. apoptotic cells to phagocytes. Nature. 2002; 417:182–187. pmid:12000961. [PubMed: 12000961]
13. Païdassi H, et al. C1q binds phosphatidylserine and likely acts as a multiligand-bridging molecule in apoptotic cell recognition. J. Immunol. 2008; 180:2329–2338. pmid:18250442. [PubMed: 18250442]
14. Lane DP. p53 guardian of the genome. Nature. 1992; 358:15–16. pmid: 1614522. [PubMed: 1614522]
15. Vogelstein B, Lane D, J A. Levine Surfing the p53 network. Nature. 2000; 408:307–310. pmid: 11099028. [PubMed: 11099028]
16. Zhivotovsky B, Kroemer G. Apoptosis and genomic instability. Nat. Rev. Mol. Cell. Biol. 2004; 5:752–762. pmid: 15340382. [PubMed: 15340382]
17. Aylon Y, Oren M. Living with p53, dying of p53. Cell. 2007; 130:597–600. pmid: 17719538. [PubMed: 17719538]
18. Kruse JP, Gu W. Modes of p53 regulation. Cell. 2009; 137:609–622. pmid: 19450511. [PubMed: 19450511]
19. Cooks T, Harris CC, Oren M. Caught in the cross fire: p53 in inflammation. Carcinogenesis. 2014; 35:1680–1690. pmid: 24942866. [PubMed: 24942866]
20. Muñoz-Fontela C, et al. Transcriptional role of p53 in interferon-mediated antiviral immunity. J. Exp. Med. 2008; 205:1929–1938. pmid: 18663127. [PubMed: 18663127]
21. Zheng SJ, Lamhamedi-Cherradi SE, Wang P, Xu L, Chen YH. Tumor suppressor p53 inhibits autoimmune inflammation and macrophage function. Diabetes. 2005; 54:1423–1428. pmid: 15855329. [PubMed: 15855329]
22. Park JS, et al. p53 controls autoimmune arthritis via STAT-mediated regulation of the Th17 cell/Treg cell balance in mice. Arthritis Rheum. 2013; 65:949–959. pmid: 23280308. [PubMed: 23280308]
23. Mori T, et al. Identification of the interferon regulatory factor 5 gene (IRF-5) as a direct target for p53. Oncogene. 2002; 21:2914–2918. pmid: 11973653. [PubMed: 11973653]
24. Hummer BT, Li XL, Hassel BA. Role for p53 in gene induction by double-stranded RNA. J. Virol. 2001; 75:7774–7777. pmid: 11462054. [PubMed: 11462054]

25. Taura M, et al. p53 regulates Toll-like receptor 3 expression and function in human epithelial cell lines. Mol. Cell. Biol. 2008; 28:6557–6567. pmid: 18779317. [PubMed: 18779317]
26. Jung DJ, et al. Foxp3 expression in p53-dependent DNA damage responses. J. Biol. Chem. 2010; 285:7995–8002. pmid: 20075077. [PubMed: 20075077]
27. Kawashima H, et al. Tumor suppressor p53 inhibits systemic autoimmune diseases by inducing regulatory T cells. J. Immunol. 2013; 191:3614–3623. pmid: 24006461. [PubMed: 24006461]
28. Lujambio A, et al. Non-cell-autonomous tumor suppression by p53. Cell. 2013; 153:449–460. pmid:23562644. [PubMed: 23562644]
29. Okuda Y, Okuda M, Bernard CC. Regulatory role of p53 in experimental autoimmune encephalomyelitis. J. Neuroimmunol. 2003; 135:29–37. pmid : 12576221. [PubMed: 12576221]
30. Zhang S, et al. Trp53 negatively regulates autoimmunity via the STAT3-Th17 axis. FASEB J. 2011; 25:2387–2398. pmid: 21471252. [PubMed: 21471252]
31. Takatori H, Kawashima H, Suzuki K, Nakajima H. Role of p53 in systemic autoimmune diseases. Crit. Rev. Immunol. 2014; 34:509–516. pmid: 25597313. [PubMed: 25597313]
32. Fray MA, Bunnell SC. p53 keeps bystanders at the gates. Immunity. 2014; 40:633–635. pmid: 24837097. [PubMed: 24837097]
33. Campbell HG, et al. Does Δ133p53 isoform trigger inflammation and autoimmunity? Cell Cycle. 2012; 11:446–450. pmid: 22262184. [PubMed: 22262184]
34. Watanabe M, Moon KD, Vacchio MS, Hathcock KS, Hodes RJ. Downmodulation of tumor suppressor p53 by T cell receptor signaling is critical for antigen-specific CD4(+) T cell responses. Immunity. 2014; 40:681–691. pmid: 24792911. [PubMed: 24792911]
35. Brown L, et al. CDIP, a novel pro-apoptotic gene regulates TNFalpha-mediated apoptosis in a p53-dependent manner. EMBO J. 2007; 26:3410–3422. pmid: 17599062. [PubMed: 17599062]
36. Sakr MA, et al. GI24 enhances tumor invasiveness by regulating cell surface membrane-type 1 matrix metalloproteinase. Cancer Sci. 2010; 101:2368–2374. pmid: 20666777. [PubMed: 20666777]
37. Wang L, et al. VISTA a novel mouse Ig superfamily ligand that negatively regulates T cell responses. J. Exp Med. 2011; 208:577–592. pmid: 21383057. [PubMed: 21383057]
38. Flies DB, Wang S, Xu H, Chen L. Cutting edge: A monoclonal antibody specific for the programmed death-1 homolog prevents graft-versus-host disease in mouse models. J. Immunol. 2011; 187:1537–1541. pmid: 21768399. [PubMed: 21768399]
39. Aloia L, Parisi S, Fusco L, Pastore L, Russo T. Differentiation of embryonic stem cells 1, (Dies1) is a component of bone morphogenetic protein 4 (BMP4) signaling pathway required for proper differentiation of mouse embryonic stem cells. J. Biol. Chem. 2010; 285:7776–7783. pmid: 20042595. [PubMed: 20042595]
40. Su AI, et al. A gene atlas of the mouse and human protein-encoding transcriptomes. Proc. Natl. Acad. Sci. U.S.A. 2004; 101:6062–6067. pmid: 15075390. [PubMed: 15075390]
41. Wu C, et al. BioGPS: An extensible and customizable portal for querying and organizing gene annotation resources. Genome Biol. 2009; 10:R130. pmid: 19919682. [PubMed: 19919682]
42. Suzuki J, Denning DP, Imanishi E, Horvitz HR, Nagata S. Xk-related protein 8 and CED-8 promote phosphatidylserine exposure in apoptotic cells. Science. 2013; 341:403–406. pmid: 23845944. [PubMed: 23845944]
43. Jeffers JR, et al. Puma is an essential mediator of p53-dependent and -independent apoptotic pathways. Cancer Cell. 2003; 4:321–328. pmid: 14585359. [PubMed: 14585359]
44. Elliott MR, et al. Nucleotides released by apoptotic cells act as a find-me signal to promote phagocytic clearance. Nature. 2009; 461:282–286. pmid: 19741708. [PubMed: 19741708]
45. Park D, et al. Continued clearance of apoptotic cells critically depends on the phagocyte Ucp2 protein. Nature. 2011; 477:220–224. pmid: 21857682. [PubMed: 21857682]
46. Fadeel B, et al. Phosphatidylserine exposure during apoptosis is a cell-type-specific event and does not correlate with plasma membrane phospholipid scramblase expression. Biochem. Biophys. Res. Commun. 1999; 266:504–511. pmid:10600532. [PubMed: 10600532]
47. Fadok VA, de Cathelineau A, Daleke DL, Henson PM, Bratton DL. Loss of phospholipid asymmetry and surface exposure of phosphatidylserine is required for phagocytosis of apoptotic

cells by macrophages and fibroblasts. J. Biol. Chem. 2001; 276:1071–1077. pmid: 10986279. [PubMed: 10986279]

48. Wang L, et al. Disruption of the immune-checkpoint VISTA gene imparts a proinflammatory phenotype with predisposition to the development of autoimmunity. Proc. Natl. Acad. Sci. USA. 2014; 111:14846–14851. pmid: 25267631. [PubMed: 25267631]
49. Flies DB, et al. Coinhibitory receptor PD-1H preferentially suppresses $CD4^+$ T cell-mediated immunity. J. Clin. Invest. 2014; 124:1966–1975. pmid: 24743150. [PubMed: 24743150]
50. O'Callaghan CA. Renal manifestations of systemic autoimmune disease: Diagnosis and therapy. Best. Pract. Res. Clin. Rheumatol. 2004; 18:411–427. pmid:15158748. [PubMed: 15158748]
51. Le Mercier I, et al. VISTA regulates the development of protective antitumor immunity. Cancer Res. 2014; 74:1933–1944. pmid: 24691994. [PubMed: 24691994]
52. Lines JL, Sempere LF, Broughton T, Wang L, Noelle R. VISTA is a, novel broad-spectrum negative checkpoint regulator for cancer immunotherapy. Cancer Immunol Res. 2014; 2:510–517. pmid: 24894088. [PubMed: 24894088]
53. Green DR, Beere HM. Apoptosis Gone but not forgotten. Nature. 2000; 405:28–29. pmid: 10811203. [PubMed: 10811203]
54. Green DR, Ferguson T, Zitvogel L, Kroemer G. Immunogenic and tolerogenic cell death. Nat. Rev. Immunol. 2009; 9:353–363. pmid: 19365408. [PubMed: 19365408]
55. Rodriguez-Manzanet R, et al. T and B cell hyperactivity and autoimmunity associated with niche-specific defects in apoptotic body clearance in TIM-4-deficient mice. Proc. Natl. Acad. Sci. USA. 2010; 107:8706–8711. pmid:20368430. [PubMed: 20368430]
56. Hanayama R, et al. Autoimmune disease and impaired uptake of apoptotic cells in MFG mice. Science. 2004; 304:1147–1150. pmid: 15155946. [PubMed: 15155946]
57. Ramirez-Ortiz ZG, et al. The scavenger receptor SCARF1 mediates the clearance of apoptotic cells and prevents autoimmunity. Nat. Immunol. 2013; 14:917–926. pmid:23892722. [PubMed: 23892722]
58. Botto M, et al. Homozygous C1q deficiency causes glomerulonephritis associated with multiple apoptotic bodies. Nat. Genet. 1998; 19:56–59. pmid: 9590289. [PubMed: 9590289]
59. Hirose Y, et al. Inhibition of Stabilin-2 elevates circulating hyaluronic acid levels and prevents tumor metastasis. Proc. Natl. Acad. Sci. U.SA. 2012; 109:4263–4268. pmid:22371575.
60. Wong K, et al. Phosphatidylserine receptor Tim-4 is essential for the maintenance of the homeostatic state of resident peritoneal macrophages. Proc. Natl. Acad. Sci. U.S.A. 2010; 107:8712–8717. pmid: 20421466. [PubMed: 20421466]
61. Fadok VA, et al. Macrophages that have ingested apoptotic cells in vitro inhibit proinflammatory cytokine production through autocrine/paracrine mechanisms involving TGF-beta, PGE2, and PAF. J. Clin. Invest. 1998; 101:890–898. pmid: 9466984. [PubMed: 9466984]
62. Fairhurst AM, Wandstrat AE, Wakeland EK. Systemic lupus erythematosus: Multiple immunological phenotypes in a complex genetic disease. Adv. Immunol. 2006; 92:1–69. pmid: 17145301. [PubMed: 17145301]
63. Liossis SN, Kovacs B, Dennis G, Kammer GM, Tsokos GC. B cells from patients with systemic lupus erythematosus display abnormal antigen receptor-mediated early signal transduction events. J. Clin. Invest. 1996; 98:2549–2557. pmid: 8958217. [PubMed: 8958217]
64. Feldman CH, et al. Epidemiology and sociodemographics of systemic lupus erytheatosus and lupus nephritis among US adults with Medicaid coverage, 2000–2004. Arthritis. Rheum. 2013; 65:753–763. pmid: 23203603. [PubMed: 23203603]
65. Li MO, Sarkisian MR, Mehal WZ, Rakic P, Flavell RA. Phosphatidylserinere receptor is required for clearance of apoptotic cells. Science. 2003; 302:1560–1563. pmid 14645847. [PubMed: 14645847]
66. Hong JR, et al. Phoshatidylserine receptor is required for the engulfment of dead apoptotic cells and for normal embryonic devopment in zebrafish. Development. 2004; 131:5417–5427. pmid: 15469976. [PubMed: 15469976]
67. QU X, et al. Autophag gene-dependent clearance of apoptotic cells during embryonic development. Cell. 2007; 128:931–946. pmid: 17350577. [PubMed: 17350577]

68. Devitt A, et al. Persisnce of apoptotic cells without autoimmune disease or inflammation in $CD14^{-/-}$ mice. J. Cell. Biol. 2004; 167:1161–1170. pmid: 15611337. [PubMed: 15611337]
69. Scott RS, et al. Phag ytosis and clearance of apoptotic cells is mediated by MER. Nature. 2001; 411:207–211. pmid: 11346799. [PubMed: 11346799]
70. Richardson L, et al. EMAGE mouse embryo spatial gene expression database: 2014 update. Nucleic. Acids. Res. 2001; 42(D1):D835–D844.
71. Arizti P, et al. Tumor suppressor p53 is required to modulate BRCA1 expression. Mol. Cell. Biol. 2000; 20:7450–7459. pmid: 11003642. [PubMed: 11003642]
72. Fang L, Li G, Liu G, Lee SW, A S. Aaronson, p53 induction of heparin-binding EGF-like growth factor counteracts p53 growth suppression through activation of MAPK and PI3K/Akt signaling cascades. EMBO J. 2001; 20:1931–1939. pmid: 11296226. [PubMed: 11296226]
73. Panigrahy D, et al. PPARalpha agonist fenofibrate suppresses tumor growth through direct and indirect angiogenesis inhibition. Proc. Natl. Acad. Sci. U.S.A. 2008; 105:985–990. pmid: 18199835. [PubMed: 18199835]
74. Ongusaha PP, et al. RhoE is a pro-survival p53 target gene that inhibits ROCK I-mediated apoptosis in response to genotoxic stress. Curr. Biol. 2006; 16:2466–2472. pmid: 17174923. [PubMed: 17174923]
75. El-Deiry WS, et al. *WAF1*, a potential mediator of p53 tumor suppression. Cell. 1993; 75:817–825. pmid: 8242752. [PubMed: 8242752]
76. Halazonetis TD, Davis LJ, Kandil AN. Wild-type p53 adopts a ‘mutant-like conformation when bound to DNA. EMBO J. 1993; 12:1021–1028. pmid: 8458320. [PubMed: 8458320]
77. Majeti R, et al. CD47 is an adverse prognostic factor and therapeutic antibody target on human acute myeloid leukemia stem cells. Cell. 2009; 138:286–299. [PubMed: 19632179]
78. Segawa K, et al. Caspase-mediated cleavage of phospholipid flippase for apoptotic phosphatidylserine exposure. Science. 2014; 344:1164–1168. pmid: 24904167. [PubMed: 24904167]
79. Jaiswal S, et al. CD47 is up regulated on circulating hematopoietic stem cells and leukemia cells to avoid phagocytosis. Cell. 2009; 138:271–285. pmid: 19632178. [PubMed: 19632178]
80. Hakroush S, et al. Effects of increased renal tubular vascular endothelial growth factor (VEGF) on fibrosis, cyst formation, and glomerular disease. Am. J. Pathol. 2009; 175:1883–1895. pmid: 19834063. [PubMed: 19834063]
81. Santiago C, et al. Structures of T Cell immunoglobulin mucin receptors 1 and 2 reveal mechanisms for regulation of immune responses by the TIM receptor family. Immunity. 2007; 26:299–310. pmid: 17363299. [PubMed: 17363299]
82. Meyers JH, et al. TIM-4 is the ligand for TIM-1, and the TIM-1-TIM-4 interaction regulates T cell proliferation. Nat. Immunol. 2005; 6:455–464. pmid: 15793576. [PubMed: 15793576]
83. Chan CJ, et al. The receptors CD96 and CD226 oppose each other in the regulation of natural killer cell functions. Nat. Immunol. 2014; 15:431–438. pmid: 24658051. [PubMed: 24658051]

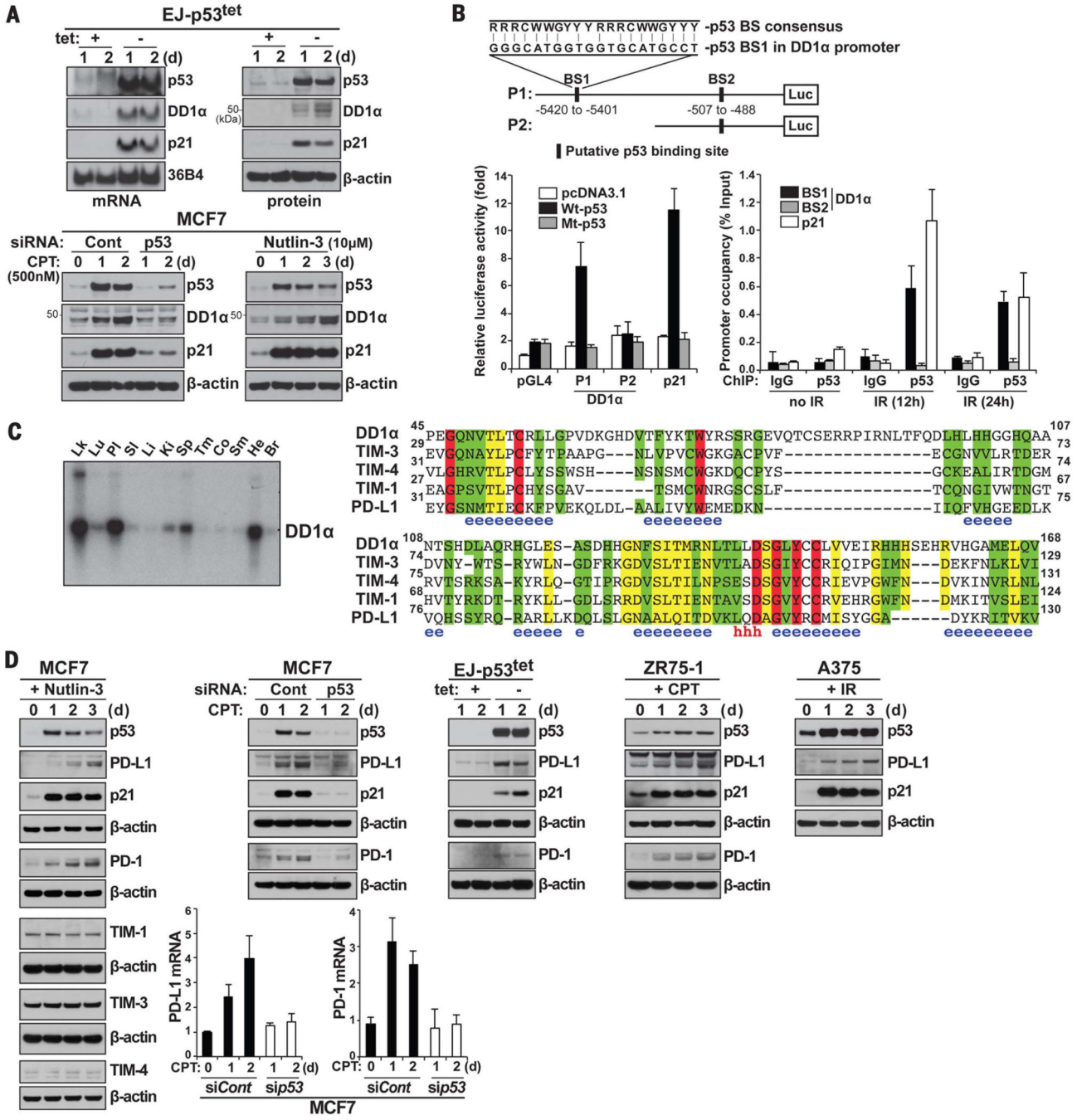

Fig. 1. Identification of *DD1α* as a p53 target gene

(**A**) p53-dependent expression of *DD1α*. *DD1α* mRNA and protein were assessed after tetracycline (tet) removal in EJ-p53^{tet} cells (tet-off) (top). MCF7 cells (bottom) were transfected with either siRNA targeting p53 or luciferase control for 24 hours, then treated with CPT (500 nM). MCF7 cells were treated with Nutlin-3 (10 μM) for the indicated times. Northern blots were used to determine mRNA expression of p53, DD1α, p21, and 36B4. Western blotting was performed with specific Abs against p53, DD1α, p21, and β-actin. (**B**) p53 binds to and transactivates the *DD1α* promoter. Luciferase reporter constructs

containing the putative p53 recognition sites in the *DD1α* promoter were cotransfected with either Wt-p53, mutant p53 (V143A), or pcDNA3.1 empty vector into U2OS cells. Results represent mean ± SD from three experiments. ChIP was performed on MCF7 cells exposed to IR (13 Gy). Immunoprecipitation was carried out with Ab against p53 (DO-1) or mouse IgG (negative control). The % input of coprecipitating DNAs was measured by qPCR and presented as mean ± SD ($n = 3$). (**C**) The expression of human *DD1α* mRNA was analyzed by Northern blotting from various human tissues, including blood leukocyte (Lk), lung (Lu), placenta (PI), small intestine (SI), liver (Li), kidney (Ki), spleen (Sp), thymus (Tm), colon (Co), skeletal muscle (Sm), heart (He), and brain (Br). Multiple sequence alignment of the IgV domains of DD1α and its homologous proteins. The predicted secondary structures are shown below the alignment as blue e for β strand and red h for α helix. The identical amino acids are in red box, the conserved amino acids are in yellow box, and the consensus amino acids are in green box. (**D**) p53-dependent expression of immune checkpoint regulators PD-1 and PD-L1. MCF7 cells were treated with 10 μM Nutlin-3 for 1 to 3 days. MCF7 cells were transfected with control siRNA or p53 siRNA for 24 hours and treated with 500 nM CPTor DMSO for 1 or 2 days. The levels of indicated proteins (TIM-1, TIM-3, TIM-4, PD-L1, and PD-1) were analyzed by Western blot analysis. Total RNAs from control siRNA or p53 siRNA transfected MCF7 cells were assessed for mRNA levels of PD-1 or PD-L1 by real-time quantitative PCR. *PD-1* or *PD-L1* mRNA levels were normalized to 36B4 expression and shown as mean ± SD ($n = 3$). ZR75-1 cells treated with 500 nM CPT or A375 cells exposed to IR (13 Gy) for indicated times.

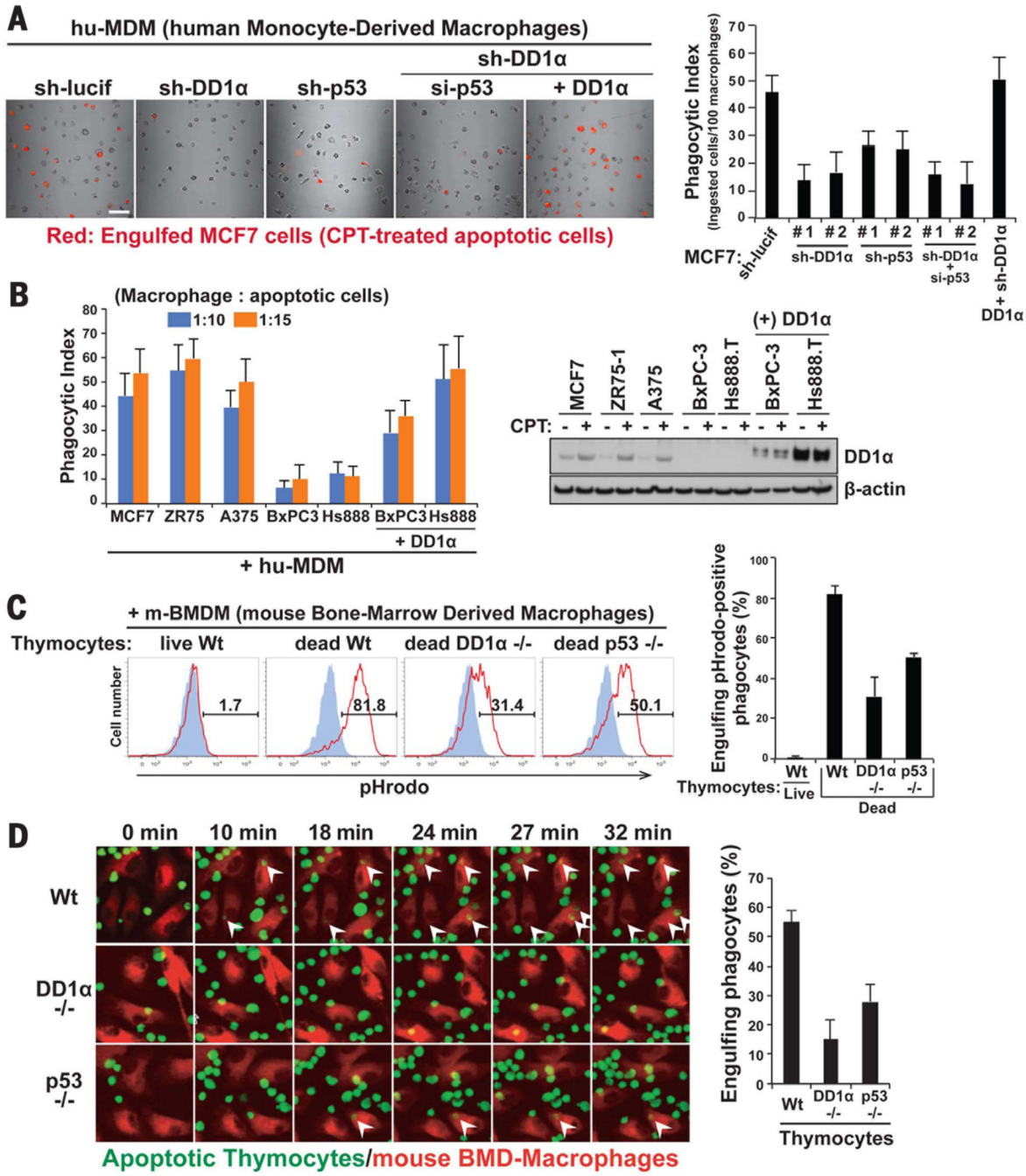

Fig. 2. DD1α plays essential roles in apoptotic cell engulfment

(**A**) DD1α on apoptotic cells contributes to apoptotic cell engulfment. MCF7 cells were transfected with shRNAs including control (luciferase) or DD1α (two different target sequences: #1, #2) or p53 (two different target sequences: #1, #2) and were treated with CPT (10 to 20 μM) for 48 hours to induce apoptosis. Then, apoptotic MCF7 cells were labeled with pHrodo, incubated with hu-MDMs for 2 hours, and examined by immunofluorescence microscopy to detect phagocytosis (red fluorescence: engulfed MCF7 cells). Where indicated, MCF7 cells expressing *DD1α* shRNA (#1) were transfected for 24 hours with

siRNA targeting p53 or a vector encoding DD1α before the phagocytosis assay. More than 400 macrophages were counted. Data are mean ± SD from three experiments. The representative images of phagocytosis with control, DD1α, p53, both *DD1*α and p53 knockdowned, and DD1α-reintroduced MCF7 cells plus hu-MDMs are shown. Scale bar, 100 μm. (**B**) Resistance of *DD1*α$^{-/-}$ cancer cells to phagocytosis. Phagocytic indices of DD1α-induced cancer cells (MCF7, ZR75-1, A375), DD1α-nonresponsive cancer cells (BxPC-3, Hs888. T), and DD1α-reintroduced DD1α-absent cancer cells (BxPC-3/DD1α, Hs888T/DD1α) were determined using hu-MDMs, as shown in Fig. 2A. The levels of DD1α protein were examined by Western blot analysis. (**C**) Engulfment of Wt, *DD1*α$^{-/-}$, and *p53*$^{-/-}$ apoptotic thymocytes by mouse bone marrow–derived macrophages (m-BMDMs) isolated from Wt mice was assessed by flow cytometry analysis. Thymocytes isolated from Wt, *DD1*α$^{-/-}$, or *p53*$^{-/-}$ mice were exposed to IR (2 to 10 Gy) to induce apoptotic populations. The pHrodo-labeled mouse thymocytes (live or apoptotic: live Wt, dead Wt, dead *DD1*α$^{-/-}$, or dead *p53*$^{-/-}$) were incubated with Wt m-BMDMs for 30 min. Phagocytosis was determined by the percentage of macrophages containing positive pHrodo signal. Data are shown as mean ± SD and representative of three independent experiments. (**D**) Engulfment of Wt, *DD1*α$^{-/-}$, and *p53*$^{-/-}$ apoptotic thymocytes by m-BMDMs was assessed by time-lapse imaging analysis. CFSE (green)–labeled apoptotic Wt, *DD1*α$^{-/-}$, or *p53*$^{-/-}$ thymocytes were incubated with PKH26 red-labeled Wt m-BMDMs. The images of phagocytosis were taken every 1 min after incubation. The representative images of engulfments were shown, and arrowheads indicate the engulfed thymocytes. Data represent mean ± SD from three different experiments.

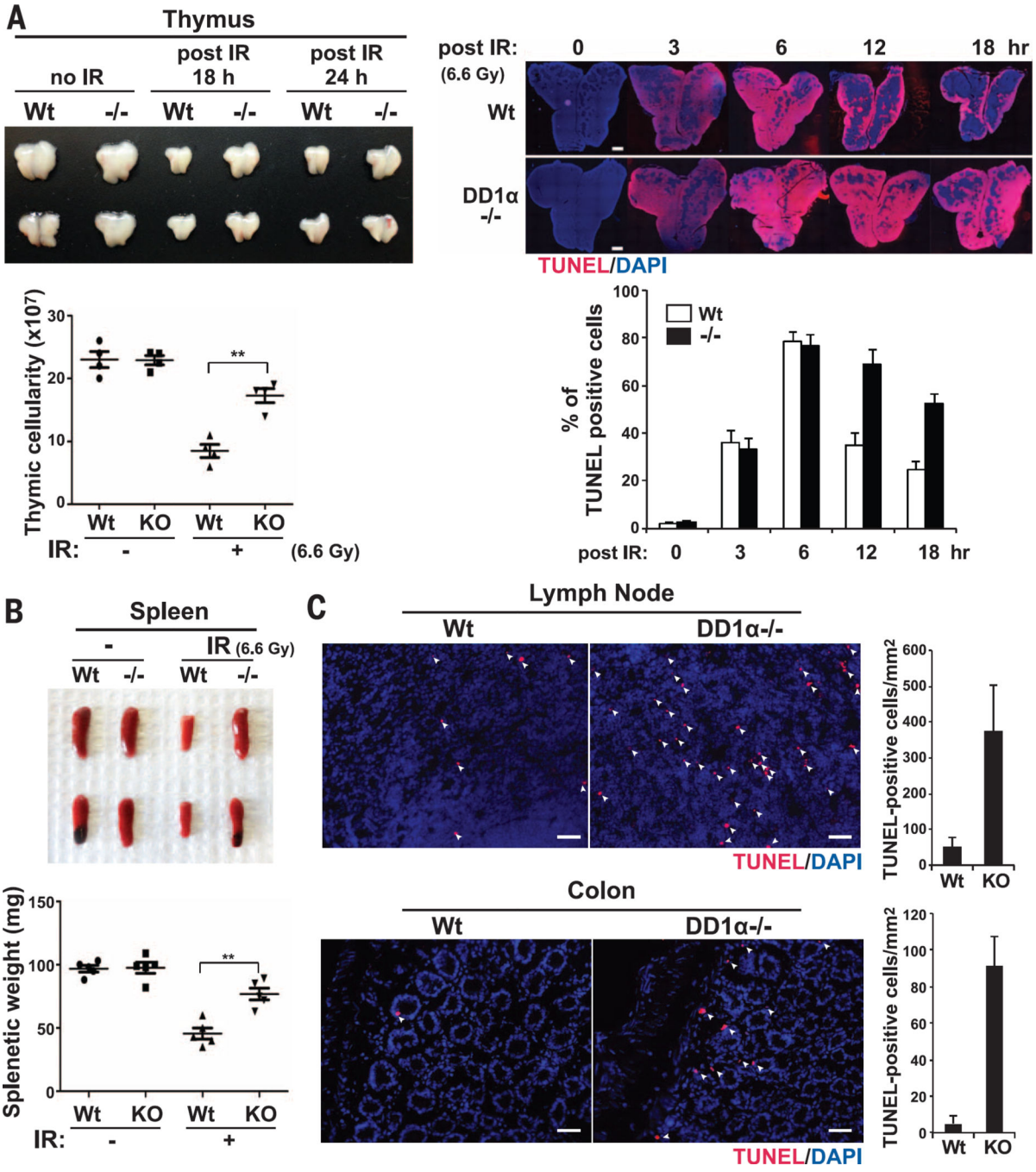

Fig. 3. Impaired clearance of apoptotic cells in the DD1α-null mice

(**A**) Photographs of representative thymus from Wt and *DD1*α$^{-/-}$ mice at indicated time points after exposure or nonexposure to IR (6.6 Gy). Total cell numbers per thymus from Wt and *DD1*α$^{-/-}$ mice were determined at 8 hours after ionizing irradiation. Mean ± SD, $n = 4$ per group. $^{**}P < 0.01$ (Tukey's test). The right panels represent whole sections of thymus from Wt and *DD1*α$^{-/-}$ mice exposed to IR that were stained with TUNEL (red) and 4′,6-diamidino-2-phenylindole (DAPI; blue). Scale bar, 1 mm. The percentage of TUNEL-positive cells was determined by percent of the TUNEL-positive cells per DAPI-positive

cells using imaging analysis program (CellSens Dimension, Olympus). Data represent mean ± SD, $n = 4$. (**B**) Spleens of Wt and *DD1*α$^{-/-}$ mice exposed to IR. Four- to five-week-old Wt and *DD1*α$^{-/-}$ mice were treated with 6.6 Gy IR. After 6 hours, spleens were isolated from mice and the splenic weight was measured. The photograph of representative spleens of Wt and *DD1*α$^{-/-}$ mice exposed to IR is shown. Each dot represents the value for a single mouse, and mean ± SD ($n = 5$) is shown. $^{**}P < 0.01$ (Tukey's test). (**C**) Apoptotic cells in lymph nodes and colon of Wt and *DD1*α$^{-/-}$ mice. The cryosections were stained with TUNEL and DAPI. The apoptotic cells were determined by counting TUNEL-positive cells per mm^2 under a fluorescence microscope. Mean ± SD, $n = 3$. Scale bar, 50 μm.

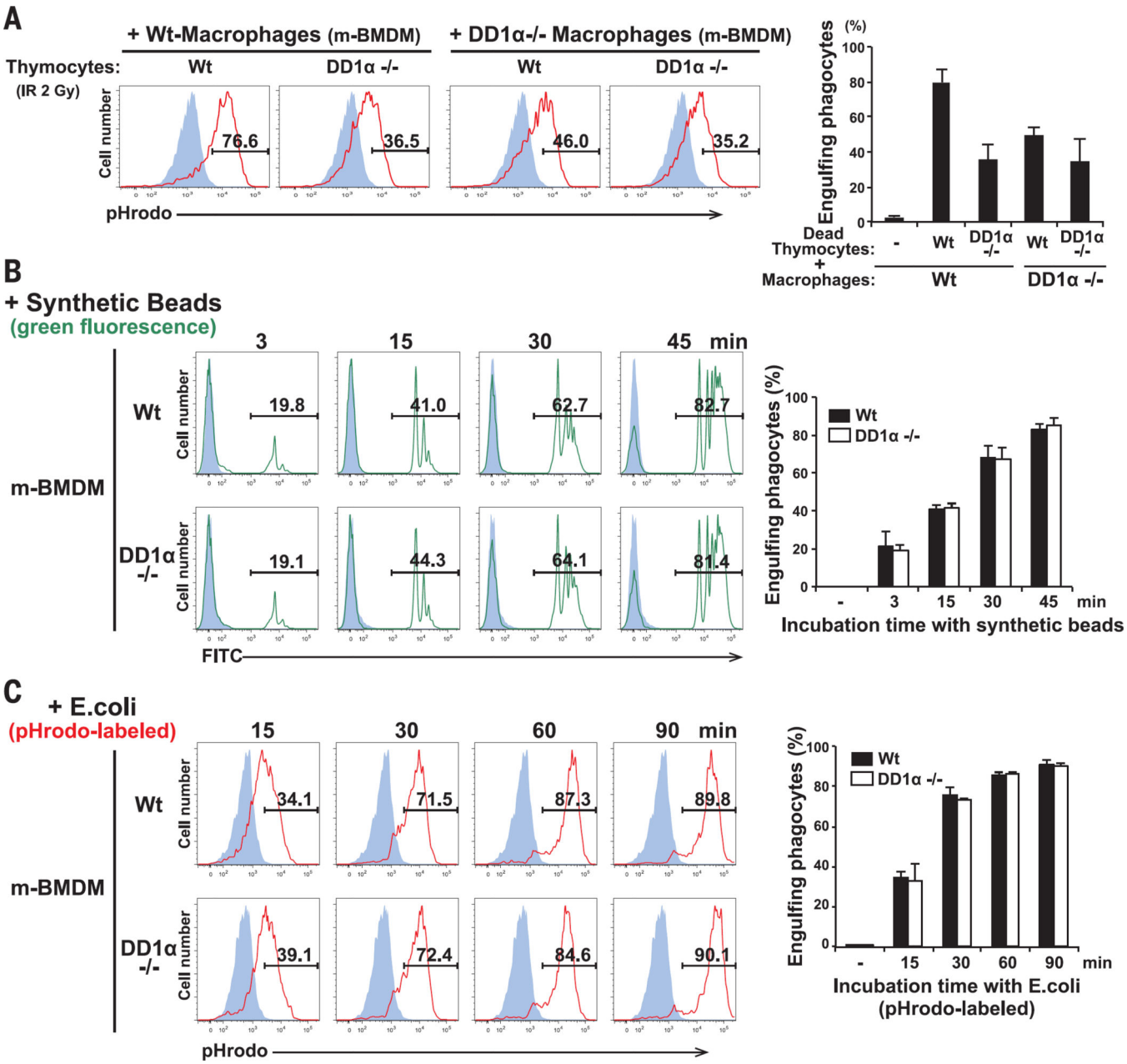

Fig. 4. DD1α expression on macrophages is required for apoptotic cell engulfment

(**A**) Engulfments of apoptotic thymocytes by Wt and *DD1*α$^{-/-}$ m-BMDMs were assessed by flow cytometry. The pHrodo-labeled apoptotic thymocytes were incubated with m-BMDMs for 30 min, and the phagocytosis was determined by measuring the positive pHrodo-containing macrophages. Graph represents mean ± SD from three experiments. (**B**) DD1α deficiency in macrophages does not influence engulfment of synthetic beads. Bone marrow–derived macrophages (m-BMDM) from Wt and *DD1*α$^{-/-}$ mice were incubated with carboxylate-modified green fluorescent beads (synthetic beads) for indicated times. The phagocytosis was determined by the percentage of macrophages containing positive green fluorescence signal. Data are shown as mean ± SD and are representative of three

experiments at the same time. (**C**) The phagocytic potential of Wt and *DD1*α$^{-/-}$ m-BMDMs for *E. coli* was assessed using pHrodo-labeled *E. coli*. The phagocytosis was determined by the percentage of macrophages containing positive pHrodo signal. Data represent mean ± SD (n = 3) and are representative of three experiments at the same time.

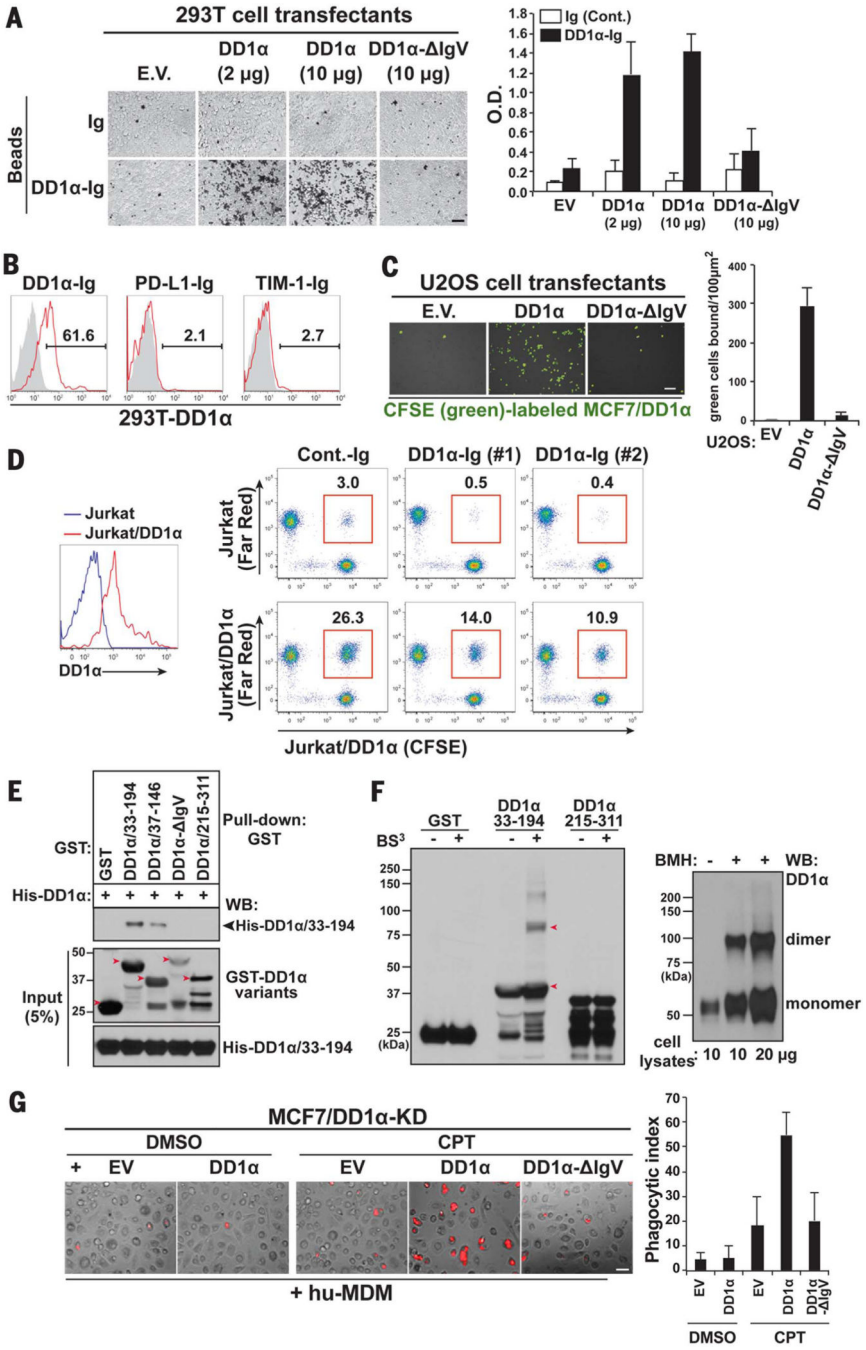

Fig. 5. Intercellular homophilic DD1α interaction between apoptotic cells and phagocytes mediates apoptotic cell engulfment

(**A**) Homophilic DD1α interaction. Binding of blue latex beads coated with DD1α-Ig fusion proteins (the extracellular region of DD1α fused with the immunoglobulin G Fc segment) to 293T cells transfected with empty vector (EV), the Wt DD1α (2 or 10 μg), or a mutant lacking the IgV domain (DD1α-ΔIgV). Ig protein–coated beads were included as control. After 30 min, unbound beads were washed. The binding was examined under an inverted microscope (left) and also determined from the optical density (O.D.) at 492 nm (right). Data are shown as mean ± SD and are representative of three experiments. Scale bar, 50 μm.

(**B**) Interaction of DD1α with DD1α on the cell surface. 293T cells stably transfected with DD1α cDNA were stained with DD1α-Ig, PD-L1–Ig, TIM-1-Ig, or control Ig proteins (gray filled). The binding of Ig proteins was detected with Ab against human IgG1-PE. Binding amounts were determined by percentage of fluorescence-positive cells compared with control Ig protein–bound cells. (**C**) Intercellular DD1α interaction. Binding of CFSE-labeled DD1α-overexpressing apoptotic MCF7 cells to U2OS cells expressing empty vector (EV), full-length DD1α, or DD1α-ΔIgV (IgV deletion mutant). Scale bar, 100 μm. Binding was determined by counting the bound cells per 100 μm^2 and normalized by cell number bound to untreated plate. Mean ± SD of three experiments is shown. (**D**) Intercellular DD1α-DD1α interaction and the disruption by recombinant DD1α proteins. The exogenous expression of DD1α in Jurkat cells was validated by flow cytometry analysis (left). CFSE-labeled DD1α-overexpressing Jurkat cells were pre-incubated with Ig proteins (control Ig: 50 μg/ml; DD1α-Ig: 25 μg/ml for #1,50 μg/ml for #2) for 30 min and mixed with Far Red–labeled control or DD1α-overexpressing Jurkat cells. After 1-hour incubation, DD1α-DD1α-mediated intercellular bindings were analyzed by counting the percentage of CFSE-and Far Red-positive populations (right). (**E**) Mapping of binding site for homophilic DD1α interaction. His-DD1α (33–194) protein was incubated with GST-DD1α variants (the extracellular region, 33–194; the immunoglobulin domain, 37–146; IgV-deleted mutant, the cytoplasmic region, 215–311) immobilized on glutathione-agarose beads. The bead-bound His-DD1α (33–194) proteins were eluted and detected by immunoblotting using Ab against His. A portion (5%) of the input proteins for the binding reaction was also subjected to immunoblotting. (**F**) Self-association of the extracellular region of DD1α in solution. GST-DD1α (33–194), GST-DD1α (215–311), or control protein GST was untreated or treated with 2.5 mM BS^3 cross-linker for 1 hour at 4°C, and GST proteins were analyzed by Western blotting using Ab against GST (left). Dimerization of DD1α was also examined in intact cells. DD1α-transfected 293T cells were treated or untreated with 1 mM bis(maleinido)hexane (BMH) for 1 hour, and DD1α protein was analyzed by Western blotting under nonreducing condition (right). (**G**) Extracellular IgV domain is required for engulfment. DD1α, DD1α-ΔIgV (IgV-deleted DD1α mutant), and control empty vector were reintroduced into DD1α-depleted MCF7 cells, and the cells were treated with DMSO or CPT (10 μM) for 48 hours. The phagocytosis of MCF7/DD1α knocked-down cells expressing empty vector (EV), DD1α, or DD1α-ΔIgV was determined as in Fig. 2A. Graph represents mean ± SD ($n = 3$). Scale bar, 50 μm.

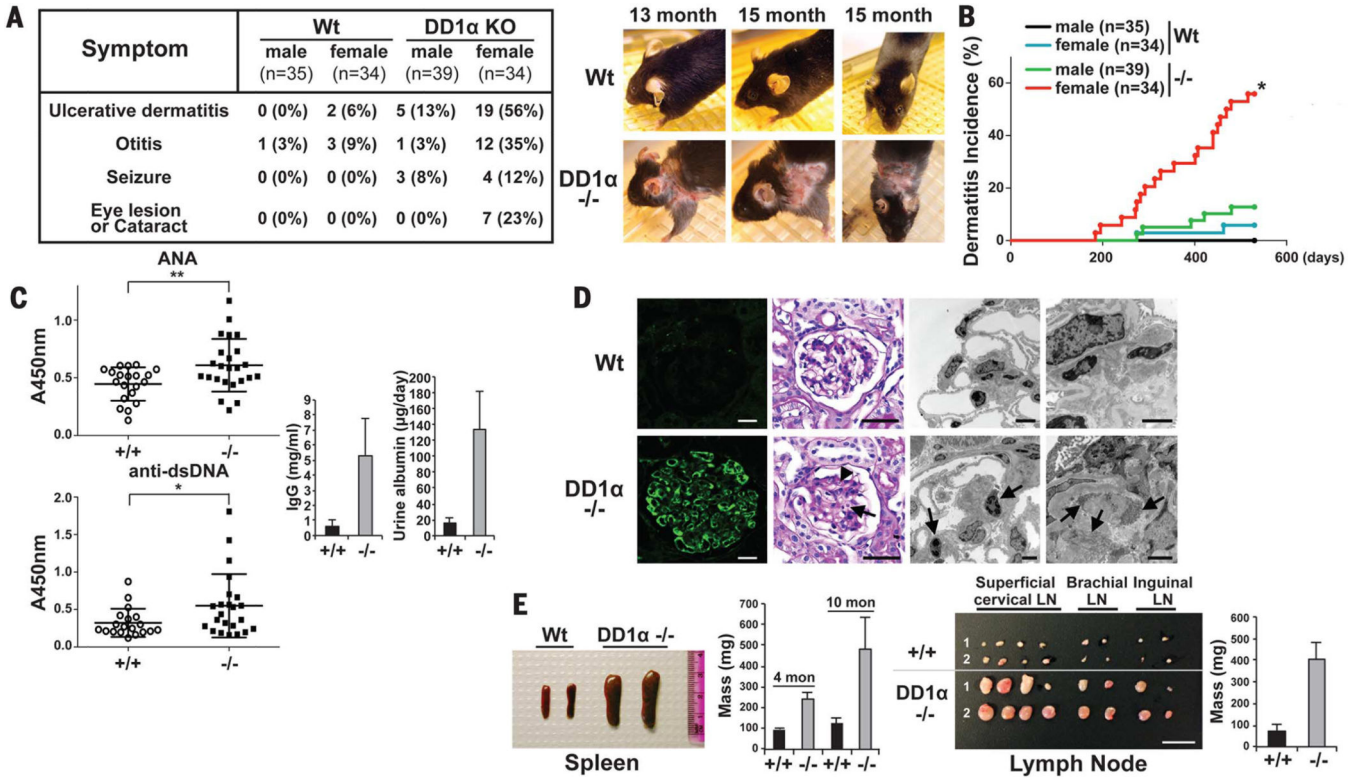

Fig. 6. DD1α-deficient mice develop autoimmune and severe inflammatory disorder

(**A**) Inflammatory phenotype of *DD1*α$^{-/-}$ mice. *DD1*α$^{-/-}$ mice (34 females, 39 males) and control Wt mice (34 females, 35 males) were observed over a 19-month period. The left box summarizes the symptoms (ulcerative dermatitis, otitis, seizure, and eye lesion) and incidences of symptoms. Photographs of 13- or 15-month-old female Wt and *DD1*α$^{-/-}$ mice are shown. (**B**) Dermatitis incidence in *DD1*α$^{-/-}$ mice (34 females and 39 males) and control Wt mice (34 females and 35 males). *$P < 0.001$ (Log-rank test). (**C**) The levels of ANA and Abs against dsDNA in sera of phenotypically affected female Wt and *DD1*α$^{-/-}$ mice were measured by ELISA. (Wt: $n = 20$, *DD1*α$^{-/-}$ $n = 24$ for ANA; and Wt: $n = 19$, *DD1*α$^{-/-}$: $n = 23$ for Abs against dsDNA). Each dot represents the value for a single mouse. **$P < 0.01$, *$P < 0.05$ (Student's t test). Serum IgG levels of phenotypically affected 10-month-old female Wt and *DD1*α$^{-/-}$ mice ($n = 7$) were assessed by ELISA. The level of albumin in urine collected for 24 hours from affected 10- to 12-month-old female mice ($n = 8$) was analyzed by SDS–polyacrylamide gel electrophoresis (SDS-PAGE) and imaging analysis. (**D**) Spontaneous glomerulonephritis in *DD1*α$^{-/-}$ mice. Representative images of kidney sections from 10-month-old Wt and *DD1*α$^{-/-}$ mice stained with Ab against mouse IgG show immune complex deposits in glomeruli of *DD1*α$^{-/-}$ mice (the first column of panels). Scale bar, 20 μm. The second column of panels shows kidney sections from Wt and *DD1*α$^{-/-}$ mice stained with PAS. Glomeruli from Wt mice have a regular architecture with delicate mesangium. Glomeruli from *DD1*α$^{-/-}$ mice with dermatitis symptoms show diffuse mesangial expansion by PAS-positive material and cellular debris (arrowhead), as well as occasional neutrophils within capillary lumens (arrow). Scale bar, 50 μm. The third column of panels shows low-magnification electron micrographs of Wt and *DD1*α$^{-/-}$ glomeruli. A

normal architecture with delicate mesangium and intact filtration barrier of Wt glomeruli and an expanded mesangium with electron-dense deposits, and neutrophils within capillary lumens (arrows) of *DD1*α$^{-/-}$ glomeruli are shown. Scale bar, 2 μm. The fourth column of panels show high magnification electron micrograph of the glomerular mesangium of Wt and *DD1*α$^{-/-}$ glomeruli. Large electron-dense deposits (arrows), often with tubular substructure in the glomerular mesangium of *DD1*α$^{-/-}$ glomeruli are shown. Scale bars, 2 μm (top) and 500 nm (bottom). (**E**) Splenomegaly and lymphadenopathy observed in *DD1*α$^{-/-}$ mice. Spleens and lymph nodes of 10-month-old female Wt and *DD1*α$^{-/-}$ mice from one littermate were shown. The weight of spleen and lymph nodes was measured as indicated. Data represent mean ± SD. n = 6 to ~11 mice per group.